Robust Polyion Complex Vesicles (PICsomes) based on PEO- b -Poly(Amino Acid) Copolymers Combining Electrostatic and Hydrophobic Interaction: Formation, siRNA Loading and Intracellular Delivery

Esra Aydinlioglu, Mona Abdelghani, Gaëlle Le Fer, Jan C. M. van Hest, Olivier Sandre, Sébastien Lecommandoux

Article published (in Open Access) in *Macromolecular Chemistry and Physics* (2022) DOI: 10.1002/macp.202200306

Robust polyion complex vesicles (PICsomes) based on PEO-*b*-poly(amino acid) copolymers combining electrostatic and hydrophobic interaction: formation, siRNA loading and intracellular delivery

Esra Aydinlioglu [1], Mona Abdelghani [2], Gaëlle Le Fer [1,3], Jan C. M. van Hest [2], Olivier Sandre [1,] and Sébastien Lecommandoux [1,*]*

1 Univ. Bordeaux, CNRS, Bordeaux INP, UMR 5629 Laboratoire de Chimie des Polymères Organiques (LCPO), ENSCBP 16 avenue Pey Berland, 33607 Pessac, France

2 Department of Biomedical Engineering, Institute for Complex Molecular Systems (ICMS), Eindhoven University of Technology, PO Box 513, 5600 MB Eindhoven, The Netherlands

3 Univ. Lille, CNRS, INRAE, Ecole Centrale, UMR 8207 Unité Matériaux Et Transformations (UMET), Ingénierie des Systèmes Polymères (ISP) team, 59000 Lille, France

* Correspondence: olivier.sandre@enscbp.fr, sebastien.lecommandoux@u-bordeaux.fr

Abstract: Two pairs of oppositely charged PEO-*b*-poly(amino acid) copolymers with neutral poly(ethylene oxide) block and polypeptide block composed of the hydrophobic *L*-phenylalanine (Phe) amino acid mixed with either negative *L*-glutamic acid (Glu) or positive *L*-lysine (Lys) units were synthesized. *N*-carboxyanhydride (NCA) ring opening polymerization (ROP) was performed with either PEO_{46}-NH_2 or PEO_{114}-NH_2 macroinitiators, leading respectively to PEO_{46}-*b*-P(Glu_{100}-*co*-Phe_{65}) and PEO_{46}-*b*-P(Lys_{100}-*co*-Phe_{65}), and PEO_{114}-*b*-P(Glu_{60}-*co*-Phe_{40}) and PEO_{114}-*b*-P(Lys_{60}-*co*-Phe_{40}). Polyion complexes (PIC) formed at near charge equilibrium led to vesicle formation (PICsomes), as shown by DLS, zetametry and TEM. The good stability of PICsomes, even in high salinity media, was interpreted by π-π stacking hydrophobic interactions between the Phe residues, playing the role of "physical cross-linking". These PICsomes were successfully loaded with siRNA directed against firefly luciferase enzyme expression. They also exhibit minimal cell cytotoxicity while superior silencing efficacy was shown by cell bioluminescence assay as compared to free siRNA and a standard lipofectamine-siRNA complex. As such, self-assembly of oppositely charged PEO-*b*-poly(amino acids) block copolymers enabled forming PICsomes of high stability thanks to π-π interactions of the Phe co-monomer in the polypeptide block, with high potential as biocompatible nanocarriers for RNA interference.

Keywords: polypeptides; PEO-*b*-poly(amino acids) block copolymers; polyion complexes*;* ring opening polymerization; small interfering RNA.

Introduction

In recent years, polymeric vesicles have gained much interest due to their unique hollow architecture with tunable membrane properties. Vesicular compartments, which are segregated from the outer aqueous medium by a membrane, can protect bioactive materials such as proteins or nucleic acids, making them potentially useful for versatile biological applications.[1–4] However, for conventional polymeric vesicles made from amphiphilic block copolymers such as poly(acrylic acid)-*block*-polystyrene (PS) or poly(ethylene oxide)-*block*-polybutadiene, the inertness and impermeability of their membrane can hinder their use for the active delivery of water soluble bioactive molecules *via* a pure diffusive mechanism.[5,6,7] To overcome this drawback, Kataoka *et coll.* developed PICsomes, standing for "PolyIon Complex vesicles" that are prepared mostly from PEG-*b*-polypeptide block copolymers and have a unique three-layered structure with a semi-permeability character.[8] In an early study, they reported uniform size PICsomes, which were formed by mixing cationic PEG_{46}-*b*-poly(aspartamide)$_{100}$ and PEG_{46}-b-poly(aspartate)$_{100}$.[9] Among structural factors that drive formation of nanoscale sized PICsomes (instead of PIC micelles or other PIC nanoparticles),[10,11] a main control parameter was shown to be to limit the PEG weight fraction (*f*-PEG) % in the block copolymers.[12] They demonstrated that too high PEG fraction prevents the growth of PICsomes and mostly directs towards micelle formation because of the immiscibility of the two (PEG and PIC) parts, as well as large steric hindrance exerted by the PEG strands. Chemical architecture of polymers is also another parameter that needs to be taken into account for PICsome formation: Kataoka *et al*. also stated that for a more stable PIC formation, longer aliphatic side chains of the polyelectrolytes are needed to favor the formation of vesicles.[9] They also were shown stable even in harsh (*i.e.* high salinity and protein content) *in vivo* conditions and efficient to deliver water soluble bioactive

molecules such as nucleic acids, proteins[13] and enzymes.[8,14–18] PICsomes can be obtained at the nanoscale from few tens to several hundred nanometers with tunable permeability based on the covalent cross-linking degree of the vesicular membrane through amide bond formation between the –COOH and $–NH_2$ side groups of the peptides, which makes them ideal nano/microreactors for the delivery of biomacromolecules.[19,20] Thanks to their facile preparation for the encapsulation of water-soluble drugs and considering that they do not need any organic solvent to be self-assembled, PICsomes are highly suitable for biomedical studies. Moreover, the PEG chains tethered to the polypeptide blocks forming the PICsome membrane serve as inner and outer shell repulsive layers prolonging their lifetime in the blood stream.[21,22]

Originally discovered in plant biology, small interfering RNA (siRNA) is a trigger of RNA interference (RNAi), which is a post-transcriptional gene expression mechanism that gained enormous interest since 2 decades due to its potential therapeutic use, especially for antiviral and anticancer therapies, but also for treatment of cardiovascular, neurological, or infectious diseases.[23] RNAi has potential therapeutic applications based on selective degradation of a target messenger RNA (mRNA) in mammalian cell cytoplasm.[23,24] But due to its fragility and high negative charge density, its bioavailability is limited as ascribed to rapid degradation by nuclease enzymes, causing inefficient cellular uptake.[25–27] Thus delivery vehicles are needed for an efficient and targeted delivery of siRNA to the cell cytoplasm. One possibility offered by the highly negatively charged repeating phosphate groups of siRNAs consists in neutralizing it through polyion complexation with oppositely charged macromolecules. Efficient candidates to do so are block copolymers combining polycationic and neutral (usually PEG) blocks, co-assembling with siRNA and providing a neutral protective layer around it. Among various *block* or *stat* copolymer architectures proposed so far in literature to form PIC assemblies with siRNA

or mRNA as potential nanomedicines[28] – for example, polyaspartamide derivatives PAsp(DET), PAsp(DPT), and PAsp(TEP),[29,30]oligosaccharide (chitosan)-*b*-PEO,[31] poly(alkyl-*L*-glutamine) copolymers,[32] diblock elastin like polypeptides (ELPs)[33,34], linear[35] or branched[36] PEG-*b*-poly(*L*-lysine) – PICsomes offer the additional advantage of possible co-encapsulation with other soluble cargos, such vesicular nanocarriers being named "siRNAsomes".[37] Another feature to consider about siRNA is that it has a rigid cylindrical structure with a length around 6 nm.[24,38] Kataoka *et al.* investigated the mechanisms of self-assembly by polyionic complexation between PEG-*b*-PLys and either single stranded (ssRNA) or double stranded siRNA. Multimolecular self-assembly (*i.e.* micellization) was strongly affected as ascribed to the rigidity of siRNA compared to ssRNA. As a consequence, siRNA and PEG-*b*-PLys form bimolecular PICs rather than larger multimolecular assemblies, at a wide range of concentrations. Thus to form multimolecular assemblies, additional attractive forces such as hydrophobic interactions and hydrogen bonds are needed within the polycationic segments to improve the driving force of complexation and reach superior transfection capability for the delivery of siRNA.[39,40] As an example, Kataoka *et al.* developed A-B-C type triblock copolymers featuring shell-forming A-segment, nucleic acid-loading B-segment, and stable core forming C-segment, directing toward construction of a three-layered polymeric micelle that can act as siRNA vehicle. These triblock copolymers were composed of hydrophilic and neutral poly(ethylene glycol) (PEG), polycationic poly(*L*-lysine) (PLys), and poly(*N*-(*N*-(2-aminoethyl)-2-aminoethyl) aspartamide) (PAsp(DET)) bearing a hydrophobic dimethoxy nitrobenzyl ester (DN) moiety in the side group. Such triblock copolymer with hydrophobic moieties showed stable encapsulation of siRNA in serum-containing medium with strong sequence-specific gene silencing effect in cultured cancer cells.[30] In another study, phenylboronic acid (PBA) functionalized cationic PIC micelles were used for

intracellular ATP-triggered release of siRNAs. The strength of the ribose–PBA binding force and the hydrophobicity of PBA, both critical determinants of complex stability, as well as the ATP sensitivity, were shown to be controllable on the basis of the substituent group structures.[41] As a last example, PEG_{114}-poly(*L*-Glu_{10}-*co*-*L*-Phe_{10}) and PEG_{114}-poly(*L*-Lys_9-*co*-*L*-Phe_{10}) copolymers with oppositely charged random co-polypeptide blocks were combined to form PIC micelles exhibiting a "charge conversion mechanism" for the pH-induced delivery of doxorubicin hydrochloride (DOX·HCl). These PIC micelles have shown superior activity and reduced side toxicity compared to free DOX in A549 tumor bearing nude mice.[42]

Considering this literature context, it appears still challenging to prepare non-toxic and stable PIC micelles in physiological conditions with the ability to deliver nucleic acid derivatives efficiently. In this work, we synthetized PEO-poly(amino acids) copolymers composed of PEO_n-poly(*L*-Glu_x-*co*-*L*-Phe_y) and PEO_n-poly(*L*-Lys_x-*co*-*L*-Phe_y) with varying neutral hydrophilic fraction *f*-PEO (wt. %) and hydrophobic fraction *f*-*L*-Phe (wt. %). The self-assembly properties of each polymer were investigated individually, then the complexation of each pair of identical degrees of polymerization of PEO (*n*), of charged unit Glu or Lys (*x*) and of Phe (*y*) was studied at different [NH_3^+/COO^-] charge ratios and *f*-PEO (wt. %) repulsive ratios. The resulting polyion complex particles were studied by mono-angle dynamic light scattering (DLS), multi-angle light scattering (MALS) and transmission electron microscopy (TEM), consistently showing PICsomes structures. We also demonstrated stability of PICsomes in presence of high salt concentrations, even without any added crosslinking agent. In literature, there are many examples of poly(*L*-lysine) based siRNA loaded polyionic complexes but only few examples with tripartite particles.[43] Furthermore, these complexes were further used for the encapsulation of siRNA as possible gene transfection agent. Their gene silencing activity was studied with the

firefly luciferase activity assay on mutant bioluminescent Luc HeLa cells and compared with the classically used polycationic transfecting agent lipofectamine.

Experimental section

Materials

Methyl- and amino- terminated poly(ethylene oxide)s (mPEO-NH_2, (M_n) PEO, without spacer = 2,000 and 5,000 g·mol^{-1}) were purchased from Rapp Polymere GmbH (Tübingen, Germany) and used without further purification. γ-Benzyl-*L*-glutamate-*N*-carboxyanhydride (γ-BLG NCA), ε-trifluoroacetyl-*L*-lysine *N*-carboxyanhydride (*L*-Lys(TFA) NCA) and *L*-Phenylalanine-*N*-carboxyanhydride (Phe NCA) were purchased from Isochem (Vert-le-Petit, France). Dry DMF was obtained from a Solvent Purification System and freshly used for the polymerization. Trifluoroacetic acid (TFA, 99%), methanesulfonic acid (MSA), and potassium carbonate (K_2CO_3) were purchased from Alfa Aesar, Thermo Fisher GmbH (Karlsruhe, Germany). Diethyl ether, DMSO, anisole and methanol were used as received from Sigma Aldrich (L'Isle d'Abeau, France). Dialysis was conducted using a Spectra/Por®6 MWCO 3.5 kDa membrane (Merck Millipore, Darmstadt, Germany). Dulbecco's modified eagle medium (DMEM), HEPES buffer (pH 7.4), and phosphate buffered saline (PBS) were purchased from ThermoFisher Scientific. Small interfering RNAs (siRNA) were obtained from Eurogentec (Angers, France): Two tubes of 21-mer siRNA duplexes targeting the pGL3 firefly luciferase gene (siRNA pGL3 luciferase control, also called siRNA duplex – firefly, antisense strand: dTdT 3'overhang, and sense strand: dTdT 3' overhang, 5 nmol of duplex per tube) were used in our experiments. For the determination of efficacy of siRNA encapsulation, Quant-iT™ microRNA assay kit (Molecular Probes, Thermo Fisher) was used as described in manufacturer's protocol. CellTiter 96® AQueous One Solution

Cell Proliferation Assay (Promega) and Luciferase Assay System (Promega) were purchased for toxicity and for gene silencing activity, respectively. HeLa EGFP-Luciferase bioluminescent cell line was provided by Utrecht University.

Instrumentation

^{1}H NMR experiments were performed in deuterated trifluoroacetic acid (*d*-TFA) at 25 °C on a Bruker Avance I NMR spectrometer (Bruker BioSpin GmbH, Rheinstetten, Germany) operating at 400 MHz and equipped with a Bruker multinuclear z-gradient direct probe head capable of producing gradients in the z direction with 53.5 G·cm^{-1} strength. ^{1}H NMR spectra were recorded with an acquisition time of 4 sec, a relaxation delay of 1-2 sec and 64 scans.

Size exclusion chromatography (SEC) was used to determine the apparent number-average molar masses (M_n) and dispersities ($Đ$) using dimethylformamide (DMF + lithium bromide (LiBr) 1g·L^{-1}) as eluent. Measurements in DMF were performed on an Ultimate 3000 system from Thermo Fisher Scientific equipped with a diode array detector (DAD) and a differential refractive index (dRI) detector (Optilab™, Wyatt Technology, Santa Barbara CA, USA). Polymers were separated on two KD-803 Shodex™ gel columns (300 × 8 mm) (exclusion limits from 1000 Da to 50 000 Da) at a flowrate of 0.8 mL·min^{-1} and column temperature held at 50°C. A series of polystyrene standards was used as the calibration. For certain copolymers synthesized from PEO_{46}-NH_2 macroinitiator, the SEC measurements were performed using dimethysulfoxide (DMSO + 0.1% LiBr) as eluent instead. In that case polymers were separated on Tosoh TSK G3000HHR and G2000HHR (7.8×300) columns (exclusion limits from 200 Da to 60 000 Da) at a flowrate of 0.5 mL·min^{-1} and column temperature held at 80°C. A dextran series was used as the calibration standard.

Mono-angle dynamic light scattering (DLS) measurements were performed on a NanoZS90 Zetasizer™ (ZEN3690, Malvern Instruments, Malvern, UK) operating with a He-Ne laser source at the wavelength of 633 nm and scattering angle of 90° at a constant central position in the cuvette (constant scattering volume). The provider's software was used to obtain *Z*-average hydrodynamic radii or diameters and polydispersity indexes (PDI) by analyzing the autocorrelation functions $g_1(t)$ in terms of relaxation time distribution $P(\tau)$ (Equation 1) and using the 2nd order cumulant method.[44]

$$g_1(t) = \int P(\tau) \exp\left(\frac{-t}{\tau}\right) d\tau = e^{\langle\Gamma\rangle t}\left[1 + \frac{\mu_2}{2!} + \cdots\right] \quad (1)$$

Hydrodynamic radius (R_h) was determined from the Stokes-Einstein relation (Equation 2).

$$R_h = k_B T / 6\pi\eta_s D_0 \quad \text{from} \quad \langle\Gamma\rangle = D_0 q^2 \quad (2a)$$

$$\text{PDI} = \mu_2 / \langle\Gamma\rangle^2 \quad (2b)$$

where D_0 is the diffusion coefficient, PDI is the polydispersity index, η_s is the viscosity of the solvent, T is the absolute temperature and k_B the Boltzmann constant.

Multi-angle light scattering (MALS) measurements were performed using an ALV/CG-6-8F compact goniometer, with a 35 mW red He-Ne linearly polarized laser (λ = 632.8 nm), an ALV/LSE-5004 multiple tau digital correlator and using a thermostat bath controller (20 °C). The data were acquired with the ALV correlator software, the counting time being typically 15 sec for each scattering angle. Angles ranged from 20° to 150° corresponding to scattering vectors q from 6.85×10^{-3} nm^{-1} to 2.55×10^{-2} nm^{-1}. The autocorrelation functions (g_1(t)) were analyzed in terms of a multi-modal relaxation time distribution $P(\tau)$ (Equation 1) and the hydrodynamic radius (R_h) was determined from the Stokes-Einstein relation (Equation 2), the translational diffusion constant D_0 being determined from the slope of the q^2 dependence of decay rate ($\langle\Gamma\rangle = 1/\tau = D_0 \cdot q^2$, τ being the main relaxation time deduced from the fitting of $g_1(\tau)$). Static light

scattering (SLS) data were reduced using standard procedures. The solvent intensity was subtracted from that of the sample. Absolute calibration was performed against toluene. The static light scattering data allowed to calculate the radius of gyration (R_g) determined from a Guinier plot according to Equation 3:

$$\ln\big(I(q)\big) \cong \ln(I_0) - R_g^2 q^2/3 \quad (3)$$

Zeta potential (ζ) of nanoobjects was determined on the NanoZS90 instrument by phase analysis light scattering (PALS) using the Smoluchowski approximation in different buffer solutions containing saline up to 0.15 M NaCl to mimic physiological conditions. All the measurements were at least the average of triplicate values and performed at 25 °C, in pure DI water or in saline at different NaCl concentrations.

Transmission electron microscopy (TEM) images were recorded on a Hitachi H7650 microscope working at 80 kV equipped with a GATAN Orius 11 Megapixel camera. Samples were prepared by dropping 5 µL of a 1 mg·mL^{-1} colloidal suspension onto a copper grid (200 mesh coated with an ultrathin lacey/continue carbon film (30/5-10 nm), Cu-200LD, Pacific Grid Tech, San Francisco CA, USA) enabling observation with natural contrast. Certain suspensions were analyzed with positive contrasting using either uranyl acetate (2% w/v) or phosphotungstic acid (0.75% w/v) as staining agents.

Synthesis of poly(ethylene oxide)$_n$-*b*-poly(*L*-glutamic acid$_x$-*co*-*L*-phenylalanine$_y$)

Copolymers were synthesized by ring-opening polymerization of BLG-NCA and Phe-NCA monomers with mPEO-NH_2 as macroinitiator. Deprotection of γ-benzyl *L*-glutamate (BLG) moieties of copolymers into *L*-glutamic acid (Glu) was performed subsequently as described in literature.[42,45] In a typical polymerization, PEO-NH_2 (0.11 g, 0.05 mmol, M_n=2,200 g·mol^{-1}) was dissolved in dry DMF (1 mL) after an azeotropic dehydration process with toluene, then Phe-

NCA (0.422 g, 2.2 mmol) and BLG-NCA (0.868 g, 3.3 mmol) which were weighted in a glovebox under pure argon, introduced in a flame-dried Schlenk tube, and dissolved in dry DMF (6 mL) were added under nitrogen using a syringe. After 3 days of reaction, poly(ethylene oxide)-*b*-poly(γ-benzyl-*L*-glutamate-*co*-*L*-phenylalanine) (PEO-*b*-poly(*L*-BLG-*co*-*L*-Phe)) block copolymer was purified by repeated precipitation from DMF into an excess amount of cold diethyl ether. The copolymer was dried under vacuum, dialyzed against water and freeze-dried to obtain a white powder. ^{1}H NMR (400 MHz, in *d*-TFA assigned chemical shifts δ (ppm): 2.26 and 2.68 (−C**H**$_2$−CH$_2$−CO−), 3.13 (C$_6$H$_5$−C**H**$_2$− of polyphenylalanine), 3.99 (PEO chain), 4.83 (C**H** of poly-γ-benzyl glutamate and polyphenylalanine), (C$_6$**H**$_5$−CH$_2$−), 6.82−7.01 (C$_6$**H**$_5$−) (Figures S1-S2 in Supplementary Info). In a second step, deprotection of BLG units was achieved in mild acidic conditions to afford *L*-glutamic acid without racemization.[46,47] Poly(ethylene oxide)$_{114}$-*b*-poly(*L*-BLG$_x$-*co*-*L*-phenylalanine$_y$) (500 mg, 2.28 mmol of BLG units) was dissolved in trifluoroacetic acid (TFA) (5 mL) and the reaction mixture was stirred at 0°C (ice bath). Then anisole (1 mL) and methanesulfonic acid (MSA) (5 mL) were added to the solution and the reaction mixture was stirred during 20 min at 0°C followed by stirring during 50 min at room temperature and maximum speed. The copolymer was finally precipitated in Et$_2$O and collected by centrifugation. The resulting mixture was dissolved in saturated sodium bicarbonate (NaHCO$_3$) solution to deprotonate the glutamic acid groups, dialyzed against distilled water (MWCO 3.5 kDa), and finally lyophilized to give the debenzylated polymer as a white solid fluffy polymer (typical yield 80%). ^{1}H NMR (400 MHz, TFA-*d*, chemical shifts δ (ppm): 3.40 (PEO chain), 6.82–7.11(C$_6$**H**$_5$–CH$_2$–), 2.58 (C$_6$H$_5$–C**H**$_2$– of polyphenylalanine), 4.38 (C**H** of poly(glutamic acid) and polyphenylalanine), 1.75–2.01(–C**H**$_2$– C**H**$_2$–COOH), 2.31(–CH$_2$–C**H**$_2$–COOH) (Figure S1B).

Synthesis of poly(ethylene oxide)$_n$-*b*-poly(*L*-lysine$_x$-*co*-*L*-phenylalanine$_y$)

In a first step, copolymers were synthesized by ring-opening polymerization (ROP) of ε-trifluoroacetyl-*L*-lysine *N*-carboxyanhydride (*L*-Lys(TFA) NCA) and *L*-phenylalanine *N*-carboxyanhydride (*L*-Phe NCA) monomers using mPEO-NH_2 as macroinitiator. Various [monomers]/[macroinitiator] and [*L*-Lys(TFA) NCA]/[*L*-Phe NCA] molar ratios were used to obtain copolypeptides with different block lengths and hydrophilic/lipophilic balances. Deprotection of TFA-*L*-lysine units of copolymers into *L*-lysine (Lys) was performed subsequently as described in literature.[47,48] In a typical polymerization, mPEO-NH_2 (0.11 g, 0.05 mmol, M_n=2,200 g·mol^{-1} with the spacer) was dissolved in dry DMF (1 mL) after an azeotropic dehydration process with toluene, then *L*-Phe-NCA (0.460 g, 4 mmol) and *L*-Lys(TFA) NCA (0.965 g, 6 mmol) which were previously kept in a glovebox under pure argon, introduced in a flame-dried Schlenk tube, and dissolved in dry DMF (6 mL) were added *via* a syringe under nitrogen. After 3 days of reaction at room temperature, poly(ethylene oxide)-*block*-poly(*L*-lysine(TFA)-*co*-*L*-phenylalanine) block copolymer was purified by repeated precipitation from DMF into an excess of cold diethyl ether. The copolymer was dried under vacuum, dialyzed against water and freeze-dried to obtain a white powder. ^{1}H NMR (400 MHz, TFA-*d*, chemical shifts δ (ppm): 6.91-7.40 (m, N**H**-$COCF_3$, C_6**H$_5$**-CH_2 and N**H** from peptide bonds), 4.25-4.68 (m, CO-C**H**-NH), 3,66 (s, O-C**H$_2$**-C**H$_2$** PEO block), 3.3 (s, C**H$_3$**-O-CH_2 PEO block), 3.25 (m, C**H$_2$**-NH-$COCF_3$), 2.84 (m, C_6H_5-C**H$_2$**), 1.25-1.63 (m, C**H$_2$**-C**H$_2$**-C**H$_2$**) (Figure S3B).

In a second step, deprotection of *L*-lysine(TFA) units was achieved. Poly(ethylene oxide)-*block*-poly(*L*-lysine(TFA)-*co*-*L*-phenylalanine) was dissolved in a 9:1 methanol: water mixture (10 mg·mL^{-1}) and K_2CO_3 (2 eq per lysine residue) was added. The reaction was stirred for 8 h at 50°C, and methanol was then removed under vacuum. The resulting solution (10% of original

volume) was then diluted in water (3 times the remaining volume), transferred to a 5,000 MWCO dialysis membrane, and then dialyzed against 0.10 M aqueous NaCl solution at pH 3 (HCl) for 24 h, followed by DI water for 48 hours with water bath changes twice per day. The content of the dialysis membrane was then freeze-dried to afford a white powder. ^{1}H NMR (400 MHz, TFA-*d*, chemical shifts δ (ppm): 6.30-7.30 (m, $C_6\mathbf{H_5}$-CH_2 and N**H** from peptide bonds), 3.70-4.25 (m, CO-C**H**-NH), 3,70 (s, O-C$\mathbf{H_2}$-C$\mathbf{H_2}$ PEO block), 2.80 (s, C$\mathbf{H_3}$-O-CH_2 PEO block), 2.70 (m, C$\mathbf{H_2}$-NH_3^+), 2.40-2.50 (m, C_6H_5-C$\mathbf{H_2}$), 0.5-1.40 (m, C$\mathbf{H_2}$-C$\mathbf{H_2}$-C$\mathbf{H_2}$) (Figure S2).

Formation of PICsomes and siRNA loading

For the formation of polyionic complexes, each polymer was firstly dissolved at 1 mg·mL^{-1} concentration in HEPES buffer at pH 7.4 and then mixed with their counterpart at desired molar charge ratios *Z*. The mixtures were vortexed 3 min, as described in literature.[49] For efficient complexation, overnight incubation at 300 rpm using an orbital shaker at room temperature was used. After formation, all nanoparticles were characterized by dynamic (DLS) and multi-angle light scattering (MALS), and neutralization curves *versus* molar charge ratio *Z* were determined by zeta potential measurements.

Loading of siRNA in the polymeric particles was performed by incubation of siRNA (20 µM in serum medium (Opti-MEM) with the preformed polymer complexes (also in Opti-MEM) at the designated [Amine]/[Phosphate+Carboxylate] ratios for 1-2 h at room temperature. More precisely, the charge ratios were defined as following:

$$Z = \frac{[-\mathrm{NH_3^+}]_{\mathrm{PEO}_n-\mathrm{poly(Lys}_x-co-\mathrm{Phe}_y)}}{[-\mathrm{PO_4^-}]_{\mathrm{siRNA}} + [-\mathrm{CO_2^-}]_{\mathrm{PEO}_n-\mathrm{poly(Glu}_x-co-\mathrm{Phe}_y)}} \quad (4)$$

SiRNA loaded particles were further characterized by DLS in an ultralow volume quartz cuvette (Ultra-Micro Cell 105.251-QS, Hellma Analytics).

Gel retardation assay

Gel electrophoresis was performed using 0.8% agarose gel at 95 V constant voltage for 40 min. Then the gel was visualized with SYBR Safe™ DNA gel stain (Invitrogen) with a GE ImageQuant™ 350 Imager.

Determination of the Effect of Polyionic Complexes on Cell Viability by MTS Assay

MTS assay (CellTiter 96® AQueous One Solution Cell Proliferation Assay (MTS, Promega®) was performed to confirm the cell viability after exposure to the PIC nanoparticles. Wild-type (WT) HeLa cells were seeded in DMEM medium with 10% fetal bovine serum (FBS) and placed into a 96-well plate to a final confluency of 10,000 cells/mL, and were incubated overnight at 37°C with 5% CO_2. Next day, cells were exposed to different concentrations of PIC nanoparticles. The cells were incubated for 48 h at 37° C with 5% CO_2. Afterward, the MTS assay was performed 24 h and 48 h post-exposure to the nanoparticles.

Ultraviolet–visible (UV/Vis) absorbance was recorded on a Jasco V-650 UV/Vis spectrometer at 490 nm and 293 K for the MTS assay.

In vitro luciferase gene silencing in cultured HeLa cells

Human cervical cancer cells stably expressing luciferase (HeLa-Luciferase) were seeded in 35 mm petri dishes (25,000 cells/dish) in DMEM medium containing 10% FBS and allowed to attach overnight. Then, the medium was removed and replaced with loaded PICsomes (at either 200 nM or 400 nM siRNA with charge ratios Z= [Amine]/[PO_3^-] +[COO^-] =1 or 10). For each analysis, control samples were prepared by addition of medium diluted with pure Opti-MEM instead of PICsome suspension. The added volumes of luciferin (luciferase substrate) and nanoparticles were 80 µL per 2 mL of medium. The cells were incubated with the nanoparticles

for 24 h, then the nanoparticles were removed and replaced by complete DMEM medium and incubated for another 48 hr. Gene knock-down was evaluated using the luciferase bioluminescence assay using a Spark® multimode microplate reader (Tecan, Männedorf, Switzerland).

Results and Discussion

Synthesis of oppositely charged PEO-b-poly(amino acid) copolymers

N-carboxy-α-amino-anhydride (NCA) ring-opening polymerization (ROP) is the most straightforward controlled polymerization technique enabling to obtain high molar masses polypeptides with no detectable racemization of the chiral centers. Polypeptides and hybrid materials exhibiting secondary structure and multi-functionalities have been obtained through the (co)polymerization of diverse NCA monomers.[50–52] For this study, PEO-*b*-poly(*L*-Glu-*co*-*L*-Phe) and PEO-*b*-poly(*L*-Lys-*co*-*L*-Phe) block copolymers were synthesized *via* the ROP of BLG-NCA or Lys(TFA)-NCA with Phe-NCA as co-monomer using mPEO-NH_2 as macroinitiator, followed by removal of the protecting groups (Scheme 1 and Scheme 2). The structures of the copolymers were determined by ^{1}H NMR and their apparent molar mass and dispersity (*Đ*) by SEC. For the formation of PICsomes, we chose oppositely charged PEO-*b*-poly(amino acid) copolymers of slightly different *f*-PEO and *f*-*L*-Phe ratios yet with nearly equal degrees of polymerization (DP) of the charged amino acids *L*-Glu and *L*-Lys, namely DP around 60 and 100, as seen in Table 1. The typical ^{1}H NMR spectra of the resulting copolymers (after deprotection) in deuterated DMSO-d6 (for PEO-*b*-poly(*L*-Glu-*co*-*L*-Phe)) or in $CDCl_3$ + TFA (PEO-*b*-poly(*L*-Lys-*co*-*L*-Phe)) are shown in Figures S1 and S3, respectively, where all peaks were assigned. The degrees of

polymerization and other molecular characterizations are summarized in Table 1. The M_n values of all synthesized copolymers were calculated by ^{1}H NMR spectroscopy (Figures S1 and S3). In most polymerizations, the targeted DPs were reached experimentally. For example, the conditions described in Methods (targeted DPs of 44 for *L*-Phe and 66 for BLG) led to the copolymer formula: PEO_{46}-*b*-poly(*L*-BLG_{62}-*co*-*L*-Phe_{42}). Corresponding SEC analyses (Figures S2 and S4) show that these copolymers exhibit narrow molar mass distribution ($Đ$ = 1.09 to 1.17). This narrow distribution may be attributed to the choice of starting PEO-NH_2 with also narrow molar mass distribution ($Đ$ = 1.13) and by the controlled polymerization character that was accomplished by the ROP mechanism of the NCA monomers.

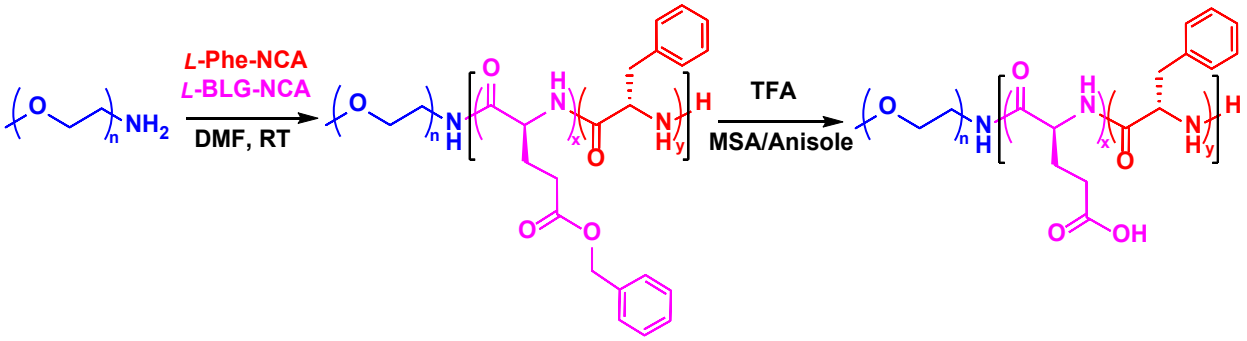

Scheme 1. Synthesis route of poly(ethylene oxide)$_n$-*b*-poly(*L*-glutamic acid$_x$-*co*-*L*-phenylalanine$_y$)

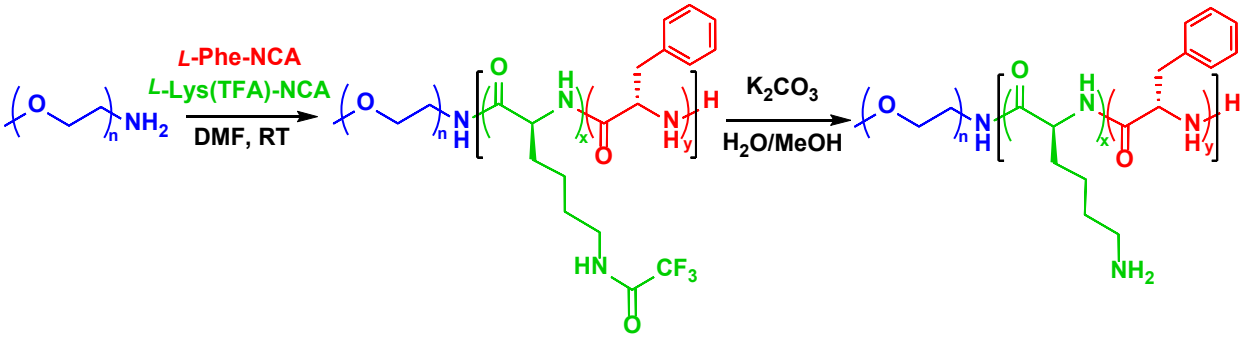

Scheme 2. Synthesis route of poly(ethylene oxide)$_n$-*b*-poly(*L*-lysine-*co*-*L*-phenylalanine$_y$)

Table 1. Molecular characteristics of the different copolymers obtained by ROP of NCA monomers at different hydrophilic weight fractions used for PICsome formations.

Copolymer	*f*-PEO (%)[a]	*f*-*L*-Phe (%)[b]	(M_n) ^{1}H-NMR (g·mol^{-1}) [c]	(M_n) SEC (g·mol^{-1}) [d]	$Đ$ [d]
PEO_{114}-*b*-poly(*L*-Glu_{60}-*co*-*L*-Phe_{36})	28	29	1.81×10^3	2.42×10^4	1.10
PEO_{114}-*b*-poly(*L*-Lys_{57}-*co*-*L*-Phe_{39})	21	25	2.34×10^4	2.77×10^4	1.11
PEO_{46}-*b*-poly(*L*-Glu_{99}-*co*-*L*-Phe_{65})	8	39	2.44×10^4	2.92×10^4 [e]	1.07
PEO_{46}-*b*-poly(*L*-Lys_{100}-*co*-*L*-Phe_{65})	6	29	3.33×10^4	4.10×10^4	1.16

[a] Hydrophilic weight fraction based on PEO content *f*-PEO (%)=(M_n^{PEO}/M_n^{tot})×100 [b] Hydrophobic weight fraction based on *L*-Phe content *f*-*L*-Phe (%)=(M_n^{PPhe}/M_n^{tot})×100 [c] Based on number of monomer units calculated by ^{1}H NMR [d] Obtained by SEC with RI detector in DMF + 0.1% LiBr *via* polystyrene calibration. [e] Obtained by SEC with RI detector in DMSO + 0.1% LiBr *via* dextran calibration (all polymers were characterized by SEC before their deprotection).

Formation and physicochemical characterizations of PICsomes

We first examined formation of PICsomes by DLS at 90° at different targeted molar ratio *Z* between NH_3^+ and COO^- moieties for the copolymers based on PEO_{46}. Zeta potential of each sample was checked at different charge ratios. Once Z was increased above one (up to 1.4), almost perfectly neutral particles were obtained, with a tendency to make large aggregates, suggesting neutralization among polymer chains and particle growth, presumably by Ostwald ripening mechanism as reported previously for PICsomes with an excess of added polycations.[53] From these DLS and zetametry results, we observed that neutralization was obtained slightly above 1:1 charge ratio, more precisely around *Z*=1.4, that might be due to a difference in the protonation state of the charged residues among the chains, PGlu and PLys being both weak electrolytes (Figure 1.a and Table 2). For the PICsome formation from PEO_{114}–based copolymers, DLS measurements were also performed at different charge ratio *Z*: Results revealed more aggregation and larger polydispersity indexes (PDI) than with PEO_{46}–based copolymers. To produce more homogeneous nanoparticles, extrusion was applied to the samples,

which is a classical method in liposome research to obtain better controlled sizes and unilamellarity.[54] For this purpose, a polycarbonate filter membrane with 200 nm well-defined, cylindrical pore channels was used. After 11 steps of extrusion, slightly better defined particles were observed for PEO_{114}–based copolymer complexes at Z=1 (Figure S5 and table S1), while the derived count rate was almost constant (meaning that negligible amount of polymers remained on the extrusion membrane). We already mentioned that f-$_{PEO}$ (%) ratio limiting is very important to design nanosized PICsomes. More detailed characterizations were performed with multi-angle light scattering (MALS) for each condition of polyionic complexation (Figure S6 and S7). MALS experiments were performed with a scattering angle varying from 20° to 150°. The linear variation of the main relaxation frequency *versus* the squared scattering vector q^2 and its passing through the origin confirm the presence of well-defined and spherical objects. MALS results also indicate possible formation of vesicles from the ratio of the radius of gyration to the hydrodynamic radius,[55] with value R_g/R_h=1.1 for PEO_{46}–based complexes and R_g/R_h=1.0 for PEO_{114}–based complexes, confirming their vesicular structure.

Table 2. Summary of results at different charge ratios after formation of polyionic complexes for PEO_{46} polymers determined by DLS.

Z ratio $[NH_3^+/COO^-]$	D_h by intensity (nm)	PDI	PDI width (nm)*	ζ potential (mV)
0.1:1	210	0.30	115	-29±5
0.5:1	170	0.30	93	-17±3
1:1	194	0.34	113	-12±7
1.4:1	2300	0.29	1240	-0.2±4

*Broadness of the size distribution determined by DLS estimated by $D_h \times \sqrt{PDI}$.[44]

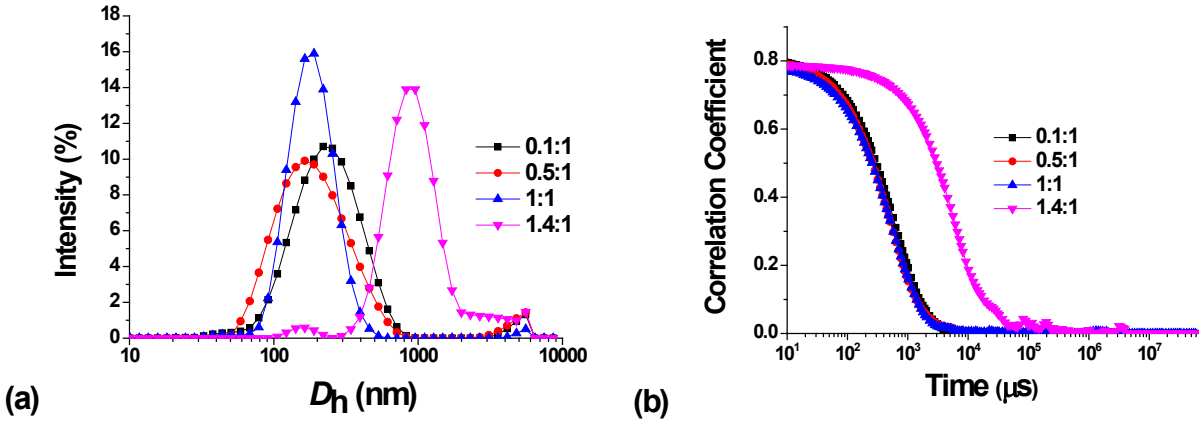

Figure 1. a) Size distribution profiles of PICsomes formed by PEO_{46}–based copolymers at different charge ratios *Z* determined from DLS measurements (Malvern, 90°). b) DLS $g_1(\tau)$ autocorrelation functions and their fitting with 2nd order Cumulant model.

TEM micrographs evidence the presence of well-dispersed spherical particles with a characteristic dark rim on the outer surface, indicating their hollow morphology (Figure 2). Since PICsomes have more fragile membranes than polymersomes, 1-ethyl-3-(3-dimethylaminopropyl) carbodiimide hydrochloride (EDC) (10 equivalents per COOH group in PEO-*b*-poly(*L*-Glu-*co*-*L*-Phe) was used to cross-link the membranes by amide bond formation to facilitate their visualization by TEM.[49,56] An average diameter of 38.5 nm (standard deviation of 9 nm) was estimated by analysis of *N*=83 particles (Figure 2). The smaller size compared to DLS is consistent with a number-weighted average diameter obtained by TEM, differing from the intensity-weighted average value determined by DLS that is more sensitive to larger sizes, reflecting the rather broad size dispersity of PICsomes (PDI around 0.3).

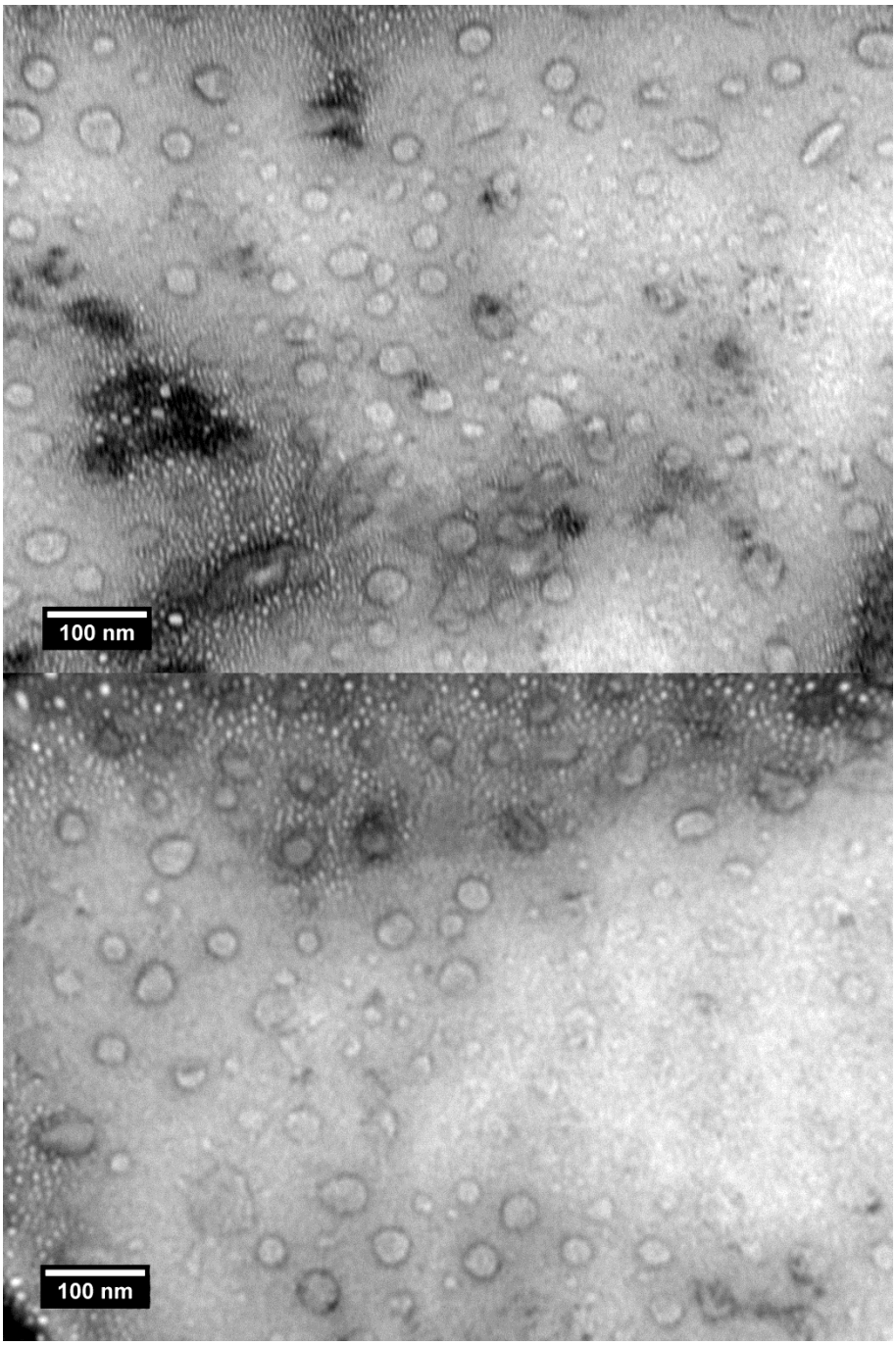

Figure 2. TEM images of PICsomes obtained from PEO_{46}–based copolymers in 10 mM PB buffer (without saline) at pH 7.4 (positively stained with 1.5% uranyl acetate solution).

Since the PEO_{46} based copolymer pair with a lower f_{PEO} (%) ratio was more favorable for complexation, we moved on to more detailed characterization with this complex. It is important

to verify the stability of polyionic complexes at physiological ionic strength and osmolarity (0.15 mM NaCl; 300 mOsm·L^{-1}) and temperature (37 °C), in order to establish if they potentially can be used for biomedical applications.[17,57] For this purpose, DLS experiments were performed at different salt concentrations, and a slight increase of the size of polyion complexes was observed, with no significant change in their PDI. Even after 1-day incubation at 37 °C with 0.15 M NaCl, the nanoparticles were neither degraded nor disassembled. At higher salt concentrations, larger sizes and PDI values were observed as ascribed to the screening of the electrostatic repulsion (Figure 3). These results indicate that the π-π interactions between *L*-Phe moieties provide enough increased stability of the PICsomes thanks to hydrophobic and aromatic interactions. The pH-dependent stability profiles of PICsomes were further characterized by DLS. The size distribution of PICsomes was clearly dependent on pH value, which may indicate the lowered association force of the PIC membranes in response to a decrease in pH, causing progressive increase in the protonation degree of the COO^- groups of glutamic acid units in the chains (Figure S8).

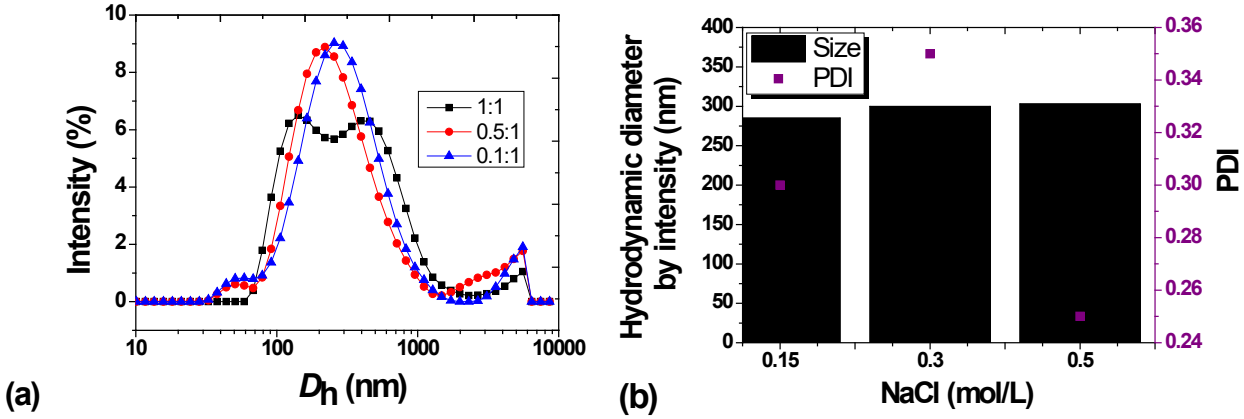

Figure 3. (a) Size distribution profiles for the stability of complexes after 1-day incubation at 37°C in 150 mM NaCl; (b) Stability against different salt concentrations at *Z*=1:1 charge ratio from DLS measurements (Malvern, 90°)

The PEO_{46}–based copolymer pair was chosen to load siRNA in its complexes since they bear around 100 charged residues in their polypeptide blocks. For this pair, both siRNA encapsulation and gene silencing activity of the complexes were studied in HeLa cells.

Formation of siRNA loaded PICsomes

The duplex – firefly double stranded oligonucleotide chosen as model siRNA was encapsulated by simple mixing with PEO_{46}-*b*-poly(*L*-Lys_{100}-*co*-*L*-Phe_{65}) and PEO_{46}-*b*-poly(*L*-Glu_{99}-*co*-*L*-Phe_{65}) copolymers. Complexation was proceeded firstly by mixing siRNA and PEO_{46}-*b*-poly(*L*-Glu_{99}-*co*-*L*-Phe_{65}), then this mixture of polyanions was subsequently complexed with a solution of PEO_{46}-*b*-poly(*L*-Lys_{100}-*co*-*L*-Phe_{65}) polycations. This complexation process was performed at various molar charge ratios Z=[N]/([P]+[COO^-]) in Opti-MEM (reduced serum medium), and each complex was analyzed by DLS and zetametry. The formation of empty PICsomes in serum media was also made and showed narrower size distributions than loaded PICsomes, besides a small secondary peak of large size aggregates (Figure S9). The siRNA loading was confirmed by gel electrophoresis for each molar ratio. The hydrodynamic size and ζ-potential of complexes were larger at higher Z ratios as observed by DLS and PALS, respectively (Figure 4). These results suggest that negatively charged siRNA strands were successfully bound to oppositely charged poly(*L*-lysine) segments in the PICsomes and that there was no macroscopic aggregation nor phase separation (coacervation), as observed when complexing with poly(*L*-Glu) polyanions only, revealing nanoscale well defined assemblies instead. Actually, charge reversal when increasing the Z ratio caused even a decrease of the hydrodynamic size of the complexes (Table 3). The complexation efficacy was studied with Quant-iT™ RiboGreen™ RNA Assay Kit using a fluorescent dye for quantification of oligonucleotides and DNA in solution.[58] While siRNA

integrated inside the particles cannot interact with the dye, only negligible amount of naked siRNA could be detected by this fluorescent labelling (Table 3). For each complex, similar levels of siRNA were targeted like in standard curves (Figure S10). Therefore, the encapsulation rates were at least 99% of the total amount of siRNA. The siRNA loading was also determined qualitatively for each ratio *via* a gel retardation assay (Figure 4d). The complete disappearance of the free siRNA band at the four studied ratios indicates that all siRNA molecules were complexed through electrostatic interactions and thus could not migrate in the agarose gel under the applied electric field. TEM images of siRNA loaded PICsomes show formation of uniform spherical nanostructures, which implies that siRNA is sandwiched between PIC membranes (Figure 5). In particular for the Z=1 charge ratio, the complexes are much monodisperse in size – average diameter of 26±6 nm counted on N=722 particles – matching their number-average diameter D_h~30-40 nm measured by DLS (Figure 4a).

Table 3. siRNA complexations at different ratios studied by DLS and their encapsulation efficacy determined by Quant-iT™ RiboGreen™ RNA Assay Kit

Z ratio [N/(P+COO^-)] N=NH_2^+ P=PO_3^-	D_h by intensity (nm)[a]	PDI[a]	EE %[b]
10	240	0.23	99
5	277	0.31	99
3	267	0.29	99
1	216	0.25	98

[a] from DLS measurements (Malvern, 90°) [b] Encapsulation efficiency of siRNA loaded PICsomes determined by Quant-iT™ RiboGreen™ RNA Assay by comparison with the standard curve (Figure S10).

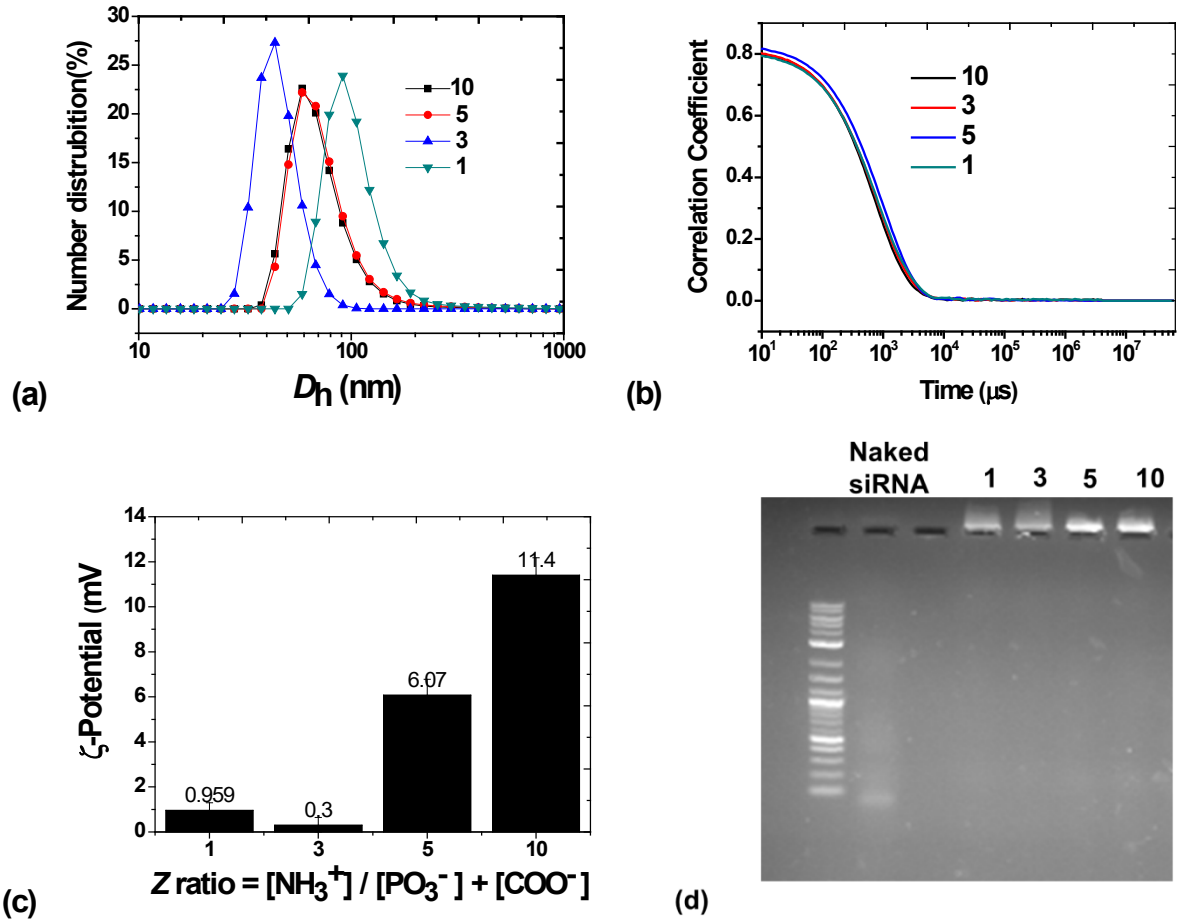

Figure 4. a) Size distribution profiles and b) $g_1(\tau)$ autocorrelograms of siRNA loaded PICsomes formed from PEO_{46} based copolymers at different charge ratios $Z = [N]/([P] + [C])$ (where N=NH_2^+, P=PO_3^-, C=COO^-) determined by DLS measurements in Opti-MEM at 37°C (Malvern, 90°); c) Zeta potential measurements; d) Gel retardation assay at different charge ratios Z=1, 3, 5 and 10.

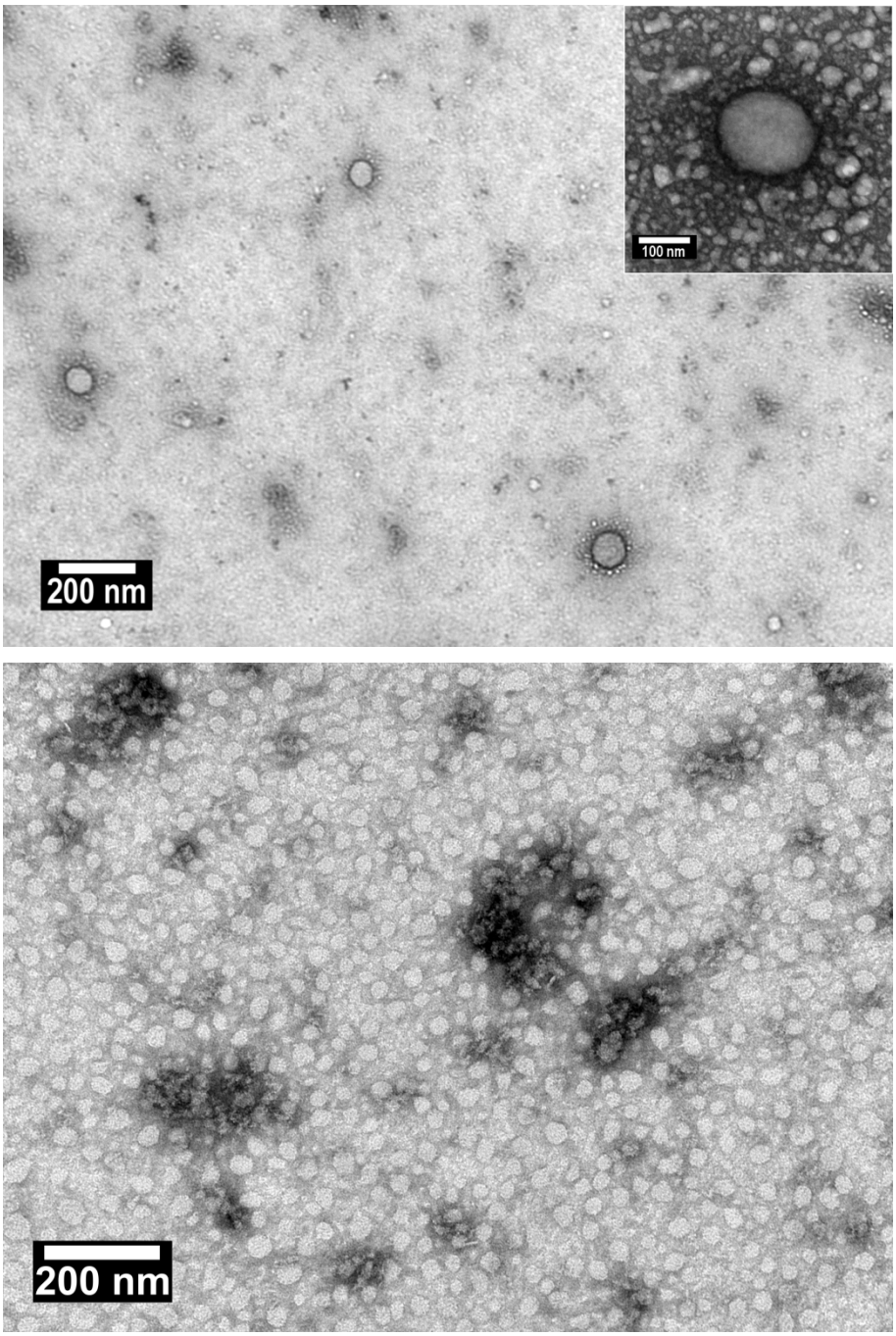

Figure 5.TEM images of siRNA loaded PICsomes: a) at [N]/([P]+[COO^-])=10 ratio (inset is a more focused image) (scale bar:100 nm); b) at [N]/([P]+[COO^-])=1 ratio (scale bar: 200 nm)

Cellular delivery of siRNA-loaded PICsomes

As a preliminary study, the gene silencing activity of siRNA loaded PICsomes was investigated in cultured human cervical cancer cells stably expressing luciferase (HeLa-Luc). An

siRNA sequence against the firefly luciferase gene was used to selectively inhibit the expression of luciferase. The commercially available Lipofectamine RNAimax was used as positive control transfection agent. The reduction in protein expression level was determined by measuring the bioluminescence using the Promega luciferase assay kit. We chose the highest and lowest [N]/([P]+[COO^-]) ratios with two different final siRNA concentrations in solution. For this purpose, the effect of PICsomes at different concentrations on cell viability was firstly determined *via* MTS assay, allowing for further gene silencing experiments. Although there was ~40% reduction of cell mitochondrial enzyme activity as measured by the MTS assay at different concentrations of cell incubation with PEO_{46}–based copolymer complexes (Figure 6), this effect did not appear to be dose-dependent, and no significant toxicity was finally observed.

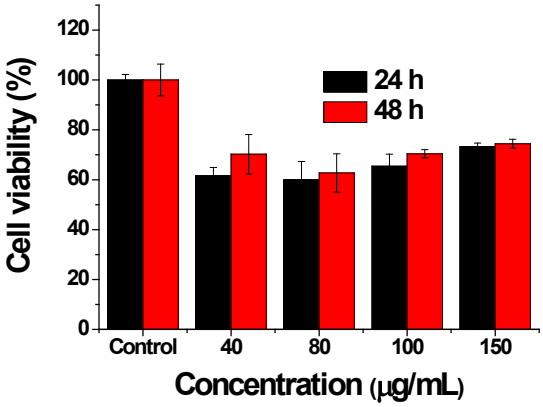

Figure 6. Percentage of cell viability of HeLa cell line after incubation with empty PEO_{46}–based PICsomes for 24 and 48 h obtained with MTS assay at several incubation concentrations.

The luciferase-based bioluminescence intensity from the cells treated with each PICsome was measured as an indicator of gene silencing. The highest siRNA concentration among PICsomes (400 nM) was also complexed with Lipofectamine™ 2000 to obtain positive control complexes that were also incubated with the cells for 24h, before gene knock-down was evaluated. These cell transfection results proved the efficiency of the siRNA loaded PICsomes (Figure 7). For

both ratios *Z*=1 and *Z*=10, PICsomes with the highest siRNA concentration (400 nM) showed that they could deliver siRNA and down-regulate the luciferin protein expression down to 20% of activity, as compared to 30% with lipofectamine.

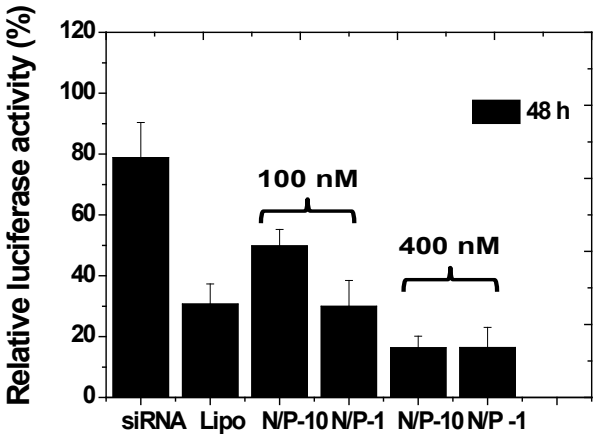

Figure 7. Relative luminescence intensity of HeLa-Luc cells incubated for 24 h with PICsomes loaded at two siRNA concentrations (100 and 400 nM) at two $Z = [N]/([P] + [C])$ ratios (*Z*=10 or 1) or with siRNA complexed with lipofectamine (at 400 nM). The bioluminescence assay was performed after 48 h. Relative luminescence intensities were obtained by normalizing to those from non-treated control cells. Results are expressed as the mean ± S.D (n=6).

Conclusion

In this study, amphiphilic copolymers with a neutral PEO block and a charged copolypeptide block of either negative, PEO-*b*-poly(*L*-Glu$_x$-*co*-*L*-Phe$_y$), or positive charge, PEO-*b*-poly(*L*-Lys$_x$-*co*-*L*-Phe$_y$), were synthesized and studied for possible PICsome formation. Different characterization methods were used to demonstrate PICsome formation at different molar charge ratios for each complex. PEO$_{46}$–based amphiphilic copolymers showed to be more favorable for the formation of PICsomes, in agreement with literature that advises to use lower molar mass PEO blocks. Moreover, stability of PICsomes in saline at 37°C was improved thanks to possible hydrophobic π-π interactions among the polypeptide chains. PICsome formulations were further

extended to be loaded with siRNA. The results revealed that PICsomes can efficiently complex siRNA through electrostatic interactions. The complexation at the highest (Z=10) and lowest (Z=1) charge ratios $Z = [\mathrm{N}]/([\mathrm{P}] + [\mathrm{C}])$ (where N=NH_2^+, P=PO_3^-, C=COO^-) with 400 nM siRNA showed more effective gene silencing activity compared to the positive control using siRNA-lipofectamine complex, with no significant toxicity. There is still a need to understand different aspects such as intracellular delivery and trafficking of these siRNA loaded PICsomes *aka* "siRNAsomes" to evaluate them as potential gene delivery agents, but these preliminary results are already very encouraging.

Author Contributions: E.A.: experiments, methodology, data collection, analysis, and writing; M.A.: experiments, data collection, and analysis; E.A, G.L.F, J. C. M. v. H, O.S. and S.L conceptualization, methodology, analysis, writing, and supervision. All authors have read and agreed to the published version of the manuscript.

Funding: This work was supported by the European Union's Horizon 2020 research and innovation programme Marie Sklodowska-Curie Innovative Training Networks (ITN) Nanomed, under grant No. 676137

Acknowledgments: The authors are grateful to Dr Anne-Laure Wirotius for ^{1}H NMR training, Amelie Wax for GPC analysis, Dr Christophe Schatz and Quentin Larger for light scattering experiments and discussions. Transmission Electron Microscopy (TEM) was performed at the Bordeaux Imaging Center, a service unit of the CNRS-INSERM and Bordeaux University, member of the national infrastructure France BioImaging; authors are grateful to Sabrina Lacomme for the TEM training sessions.

Conflicts of Interest: The authors declare no conflict of interest.

References

(1) Christian, D. A.; Cai, S.; Bowen, D. M.; Kim, Y.; Pajerowski, J. D.; Discher, D. E. Polymersome Carriers: From Self-Assembly to SiRNA and Protein Therapeutics. *Eur. J. Pharm. Biopharm.* **2009**, *71* (3), 463–474. https://doi.org/10.1016/j.ejpb.2008.09.025.

(2) Tanner, P.; Baumann, P.; Enea, R.; Onaca, O.; Palivan, C.; Meier, W. Polymeric Vesicles: From Drug Carriers to Nanoreactors and Artificial Organelles. *Acc. Chem. Res.* **2011**, *44* (10), 1039–1049. https://doi.org/10.1021/ar200036k.

(3) Lee, J. S.; Feijen, J. Polymersomes for Drug Delivery: Design, Formation and Characterization. *J. Control. Release* **2012**, *161* (2), 473–483. https://doi.org/10.1016/j.jconrel.2011.10.005.

(4) Hu, X.; Zhang, Y.; Xie, Z.; Jing, X.; Bellotti, A.; Gu, Z. Stimuli-Responsive Polymersomes for Biomedical Applications. *Biomacromolecules* **2017**, *18* (3), 649–673. https://doi.org/10.1021/acs.biomac.6b01704.

(5) Spulber, M.; Najer, A.; Winkelbach, K.; Glaied, O.; Waser, M.; Pieles, U.; Meier, W.; Bruns, N. Photoreaction of a Hydroxyalkyphenone with the Membrane of Polymersomes: A Versatile Method to Generate Semipermeable Nanoreactors. *J. Am. Chem. Soc.* **2013**, *135* (24), 9204–9212. https://doi.org/10.1021/ja404175x.

(6) Wang, X.; Liu, G.; Hu, J.; Zhang, G.; Liu, S. Concurrent Block Copolymer Polymersome Stabilization and Bilayer Permeabilization by Stimuli-Regulated "Traceless" Crosslinking. *Angew. Chemie - Int. Ed.* **2014**, *53* (12), 3138–3142. https://doi.org/10.1002/anie.201310589.

(7) Wang, X.; Yao, C.; Zhang, G.; Liu, S. Regulating Vesicle Bilayer Permeability and Selectivity via Stimuli-Triggered Polymersome-to-PICsome Transition. *Nat. Commun.*

2020, *11* (1), 1524. https://doi.org/10.1038/s41467-020-15304-x.

(8) Koide, A.; Kishimura, A.; Osada, K.; Jang, W. D.; Yamasaki, Y.; Kataoka, K. Semipermeable Polymer Vesicle (PICsome) Self-Assembled in Aqueous Medium from a Pair of Oppositely Charged Block Copolymers: Physiologically Stable Micro-/Nanocontainers of Water-Soluble Macromolecules. *J. Am. Chem. Soc.* **2006**, *128* (18), 5988–5989. https://doi.org/10.1021/ja057993r.

(9) Chuanoi, S.; Kishimura, A.; Dong, W. F.; Anraku, Y.; Yamasaki, Y.; Kataoka, K. Structural Factors Directing Nanosized Polyion Complex Vesicles (Nano-PICsomes) to Form a Pair of Block Aniomer/Homo Catiomers: Studies on the Aniomer Segment Length and the Catiomer Side-Chain Structure. *Polym. J.* **2014**, *46* (2), 130–135. https://doi.org/10.1038/pj.2013.82.

(10) Hammond, P. T. Building Biomedical Materials Layer-by-Layer. *Mater. Today* **2012**, *15* (5), 196–206. https://doi.org/10.1016/S1369-7021(12)70090-1.

(11) Insua, I.; Wilkinson, A.; Fernandez-Trillo, F. Polyion Complex (PIC) Particles: Preparation and Biomedical Applications. *Eur. Polym. J.* **2016**, *81*, 198–215. https://doi.org/10.1016/j.eurpolymj.2016.06.003.

(12) Dong, W. F.; Kishimura, A.; Anraku, Y.; Chuanoi, S.; Kataoka, K. Monodispersed Polymeric Nanocapsules: Spontaneous Evolution and Morphology Transition from Reducible Hetero-PEG PICmicelles by Controlled Degradation. *J. Am. Chem. Soc.* **2009**, *131* (11), 3804–3805. https://doi.org/10.1021/ja808419b.

(13) Kishimura, A.; Koide, A.; Osada, K.; Yamasaki, Y.; Kataoka, K. Encapsulation of Myoglobin in PEGylated Polyion Complex Vesicles Made from a Pair of Oppositely Charged Block Ionomers: A Physiologically Available Oxygen Carrier. *Angew. Chemie* -

Int. Ed. **2007**, *46* (32), 6085–6088. https://doi.org/10.1002/anie.200701776.

(14) Sueyoshi, D.; Anraku, Y.; Komatsu, T.; Urano, Y.; Kataoka, K. Enzyme-Loaded Polyion Complex Vesicles as in Vivo Nanoreactors Working Sustainably under the Blood Circulation: Characterization and Functional Evaluation. *Biomacromolecules* **2017**, *18* (4), 1189–1196. https://doi.org/10.1021/acs.biomac.6b01870.

(15) Anraku, Y.; Kishimura, A.; Yamasaki, Y.; Kataoka, K. Living Unimodal Growth of Polyion Complex Vesicles via Two-Dimensional Supramolecular Polymerization. *J. Am. Chem. Soc.* **2013**, *135* (4), 1423–1429. https://doi.org/10.1021/ja3096587.

(16) Anraku, Y.; Kishimura, A.; Kamiya, M.; Tanaka, S.; Nomoto, T.; Toh, K.; Matsumoto, Y.; Fukushima, S.; Sueyoshi, D.; Kano, M. R.; Urano, Y.; Nishiyama, N.; Kataoka, K. Systemically Injectable Enzyme-Loaded Polyion Complex Vesicles as in Vivo Nanoreactors Functioning in Tumors. *Angew. Chemie - Int. Ed.* **2016**, *55* (2), 560–565. https://doi.org/10.1002/anie.201508339.

(17) Anraku, Y.; Kishimura, A.; Oba, M.; Yamasaki, Y.; Kataoka, K. Spontaneous Formation of Nanosized Unilamellar Polyion Complex Vesicles with Tunable Size and Properties. *J. Am. Chem. Soc.* **2010**, *132* (5), 1631–1636. https://doi.org/10.1021/ja908350e.

(18) Hori, M.; Cabral, H.; Toh, K.; Kishimura, A.; Kataoka, K. Robust Polyion Complex Vesicles (PICsomes) under Physiological Conditions Reinforced by Multiple Hydrogen Bond Formation Derived by Guanidinium Groups. *Biomacromolecules* **2018**, *19* (10), 4113–4121. https://doi.org/10.1021/acs.biomac.8b01097.

(19) Kishimura, A. Development of Polyion Complex Vesicles (PICsomes) from Block Copolymers for Biomedical Applications. *Polym. J.* **2013**, *45* (9), 892–897. https://doi.org/10.1038/pj.2013.33.

(20) Bennett, K. M.; Jo, J. I.; Cabral, H.; Bakalova, R.; Aoki, I. MR Imaging Techniques for Nano-Pathophysiology and Theranostics. *Adv. Drug Deliv. Rev.* **2014**, *74*, 75–94. https://doi.org/10.1016/j.addr.2014.04.007.

(21) Hamley, I. W. PEG-Peptide Conjugates. *Biomacromolecules* **2014**, *15* (5), 1543–1559. https://doi.org/10.1021/bm500246w.

(22) Anraku, Y.; Kishimura, A.; Kobayashi, A.; Oba, M.; Kataoka, K. Size-Controlled Long-Circulating PICsome as a Ruler to Measure Critical Cut-off Disposition Size into Normal and Tumor Tissues. *Chem. Commun.* **2011**, *47* (21), 6054–6056. https://doi.org/10.1039/c1cc11465d.

(23) Elbashir, S. M.; Harborth, J.; Lendeckel, W.; Yalcin, A.; Weber, K.; Tuschl, T. Duplexes of 21-Nucleotide RNAs Mediate RNA Interference in Cultured Mammalian Cells. *Nature* **2001**, *411* (6836), 494–498. https://doi.org/10.1038/35078107.

(24) Rana, T. M. Illuminating the Silence: Understanding the Structure and Function of Small RNAs. *Nat. Rev. Mol. Cell Biol.* **2007**, *8* (1), 23–36. https://doi.org/10.1038/nrm2085.

(25) Kaczmarek, J. C.; Kowalski, P. S.; Anderson, D. G. Advances in the Delivery of RNA Therapeutics: From Concept to Clinical Reality. *Genome Medicine*. 2017, p 60. https://doi.org/10.1186/s13073-017-0450-0.

(26) Kim, H. J.; Kim, A.; Miyata, K.; Kataoka, K. Recent Progress in Development of SiRNA Delivery Vehicles for Cancer Therapy. *Adv. Drug Deliv. Rev.* **2016**, *104*, 61–77. https://doi.org/10.1016/j.addr.2016.06.011.

(27) Wittrup, A.; Lieberman, J. Knocking down Disease: A Progress Report on SiRNA Therapeutics. *Nat. Rev. Genet.* **2015**, *16* (9), 543–552. https://doi.org/10.1038/nrg3978.

(28) Sharma, A.; Jha, N. K.; Dahiya, K.; Singh, V. K.; Chaurasiya, K.; Jha, A. N.; Jha, S. K.;

Mishra, P. C.; Dholpuria, S.; Astya, R.; Nand, P.; Kumar, A.; Ruokolainen, J.; Kesari, K. K. Nanoparticulate RNA Delivery Systems in Cancer. *Cancer Rep.* **2020**, *3* (5), e1271. https://doi.org/10.1002/cnr2.1271.

(29) Suma, T.; Miyata, K.; Ishii, T.; Uchida, S.; Uchida, H.; Itaka, K.; Nishiyama, N.; Kataoka, K. Enhanced Stability and Gene Silencing Ability of SiRNA-Loaded Polyion Complexes Formulated from Polyaspartamide Derivatives with a Repetitive Array of Amino Groups in the Side Chain. *Biomaterials* **2012**, *33* (9), 2770–2779. https://doi.org/10.1016/j.biomaterials.2011.12.022.

(30) Kim, H. J.; Miyata, K.; Nomoto, T.; Zheng, M.; Kim, A.; Liu, X.; Cabral, H.; Christie, R. J.; Nishiyama, N.; Kataoka, K. SiRNA Delivery from Triblock Copolymer Micelles with Spatially-Ordered Compartments of PEG Shell, SiRNA-Loaded Intermediate Layer, and Hydrophobic Core. *Biomaterials* **2014**, *35* (15), 4548–4556. https://doi.org/10.1016/j.biomaterials.2014.02.016.

(31) Delas, T.; Mock-Joubert, M.; Faivre, J.; Hofmaier, M.; Sandre, O.; Dole, F.; Chapel, J. P.; Crépet, A.; Trombotto, S.; Delair, T.; Schatz, C. Effects of Chain Length of Chitosan Oligosaccharides on Solution Properties and Complexation with SiRNA. *Polymers (Basel).* **2019**, *11* (8), 1236. https://doi.org/10.3390/polym11081236.

(32) Klemm, P.; I. Solomun, J.; Rodewald, M.; T. Kuchenbrod, M.; G. Hänsch, V.; Richter, F.; Popp, J.; Hertweck, C.; Hoeppener, S.; Bonduelle, C.; Lecommandoux, S.; Traeger, A.; Schubert, S. Efficient Gene Delivery of Tailored Amphiphilic Polypeptides by Polyplex Surfing. *Biomacromolecules* **2022**, *23* (11), 4718–4733. https://doi.org/10.1021/acs.biomac.2c00919.

(33) Abdelghani, M.; Shao, J.; Le, D. H. T.; Wu, H.; van Hest, J. C. M. Self-Assembly or

Coassembly of Multiresponsive Histidine-Containing Elastin-Like Polypeptide Block Copolymers. *Macromol. Biosci.* **2021**, *21* (6). https://doi.org/10.1002/mabi.202100081.

(34) Bravo-Anaya, L. M.; Garbay, B.; Nando-Rodríguez, J. L. E.; Carvajal Ramos, F.; Ibarboure, E.; Bathany, K.; Xia, Y.; Rosselgong, J.; Joucla, G.; Garanger, E.; Lecommandoux, S. Nucleic Acids Complexation with Cationic Elastin-like Polypeptides: Stoichiometry and Stability of Nano-Assemblies. *J. Colloid Interface Sci.* **2019**, *557*, 777–792. https://doi.org/10.1016/J.JCIS.2019.09.054.

(35) Zhou, Z.; Yeh, C. F.; Mellas, M.; Oh, M. J.; Zhu, J.; Li, J.; Huang, R. T.; Harrison, D. L.; Shentu, T. P.; Wu, D.; Lueckheide, M.; Carver, L.; Chung, E. J.; Leon, L.; Yang, K. C.; Tirrell, M. V.; Fang, Y. Targeted Polyelectrolyte Complex Micelles Treat Vascular Complications in Vivo. *Proc. Natl. Acad. Sci. U. S. A.* **2021**, *118* (50). https://doi.org/10.1073/pnas.2114842118.

(36) Chaya, H.; Naito, M.; Cho, M.; Toh, K.; Hayashi, K.; Fukushima, S.; Yamasaki, Y.; Kataoka, K.; Miyata, K. Dynamic Stabilization of Unit Polyion Complexes Incorporating Small Interfering RNA by Fine-Tuning of Cationic Block Length in Two-Branched Poly(Ethylene Glycol)- b-Poly(l -Lysine). *Biomacromolecules* **2022**, *23* (1), 388–397. https://doi.org/10.1021/acs.biomac.1c01344.

(37) Kim, B. S.; Chuanoi, S.; Suma, T.; Anraku, Y.; Hayashi, K.; Naito, M.; Kim, H. J.; Kwon, I. C.; Miyata, K.; Kishimura, A.; Kataoka, K. Self-Assembly of SiRNA/PEG- b-Catiomer at Integer Molar Ratio into 100 Nm-Sized Vesicular Polyion Complexes (SiRNAsomes) for RNAi and Codelivery of Cargo Macromolecules. *J. Am. Chem. Soc.* **2019**, *141* (8), 3699–3709. https://doi.org/10.1021/jacs.8b13641.

(38) Hyeon, C.; Dima, R. I.; Thirumalai, D. Size, Shape, and Flexibility of RNA Structures. *J.*

Chem. Phys. **2006**, *125* (19), 194905. https://doi.org/10.1063/1.2364190.

(39) Kim, H. J.; Ishii, T.; Zheng, M.; Watanabe, S.; Toh, K.; Matsumoto, Y.; Nishiyama, N.; Miyata, K.; Kataoka, K. Multifunctional Polyion Complex Micelle Featuring Enhanced Stability, Targetability, and Endosome Escapability for Systemic SiRNA Delivery to Subcutaneous Model of Lung Cancer. *Drug Deliv. Transl. Res.* **2014**, *4* (1), 50–60.

(40) Kataoka, K.; Harada, A.; Nagasaki, Y. Block Copolymer Micelles for Drug Delivery: Design, Characterization and Biological Significance. *Adv. Drug Deliv. Rev.* **2012**, *64* (SUPPL.), 37–48. https://doi.org/10.1016/j.addr.2012.09.013.

(41) Naito, M.; Ishii, T.; Matsumoto, A.; Miyata, K.; Miyahara, Y.; Kataoka, K. A Phenylboronate-Functionalized Polyion Complex Micelle for ATP-Triggered Release of SiRNA. *Angew. Chemie - Int. Ed.* **2012**, *51* (43), 10751–10755. https://doi.org/10.1002/anie.201203360.

(42) Lv, S.; Song, W.; Tang, Z.; Li, M.; Yu, H.; Hong, H.; Chen, X. Charge-Conversional Peg-Polypeptide Polyionic Complex Nanoparticles from Simple Blending of a Pair of Oppositely Charged Block Copolymers as an Intelligent Vehicle for Efficient Antitumor Drug Delivery. *Mol. Pharm.* **2014**, *11* (5), 1562–1574. https://doi.org/10.1021/mp4007387.

(43) Boudier, A.; Aubert-Pouëssel, A.; Gérardin, C.; Devoisselle, J. M.; Bégu, S.; Louis-Plence, P.; Quentin, J.; Jorgensen, C. Tripartite SiRNA Micelles as Controlled Delivery Systems for Primary Dendritic Cells. *Drug Dev. Ind. Pharm.* **2009**, *35* (8), 950–958. https://doi.org/10.1080/03639040802716653.

(44) Johnson, C. S.; Gabriel, D. A. Laser Light Scattering. In *Spectroscopy in Biochemistry*; CRC Press, 2018; pp 177–248. https://doi.org/10.1201/9781351076814-5.

(45) Lv, S.; Li, M.; Tang, Z.; Song, W.; Sun, H.; Liu, H.; Chen, X. Doxorubicin-Loaded Amphiphilic Polypeptide-Based Nanoparticles as an Efficient Drug Delivery System for Cancer Therapy. *Acta Biomater.* **2013**, *9* (12), 9330–9342. https://doi.org/10.1016/j.actbio.2013.08.015.

(46) Bonduelle, C.; Makni, F.; Severac, L.; Piedra-Arroni, E.; Serpentini, C. L.; Lecommandoux, S.; Pratviel, G. Smart Metallopoly(l-Glutamic Acid) Polymers: Reversible Helix-to-Coil Transition at Neutral PH. *RSC Adv.* **2016**, *6* (88), 84694–84697. https://doi.org/10.1039/c6ra19753a.

(47) Sun, Y.; Wollenberg, A. L.; O'Shea, T. M.; Cui, Y.; Zhou, Z. H.; Sofroniew, M. V.; Deming, T. J. Conformation-Directed Formation of Self-Healing Diblock Copolypeptide Hydrogels via Polyion Complexation. *J. Am. Chem. Soc.* **2017**, *139* (42), 15114–15121. https://doi.org/10.1021/jacs.7b08190.

(48) Rodríguez-Hernández, J.; Gatti, M.; Klok, H. A. Highly Branched Poly(L-Lysine). *Biomacromolecules* **2003**, *4* (2), 249–258. https://doi.org/10.1021/bm020096k.

(49) Chuanoi, S.; Anraku, Y.; Hori, M.; Kishimura, A.; Kataoka, K. Fabrication of Polyion Complex Vesicles with Enhanced Salt and Temperature Resistance and Their Potential Applications as Enzymatic Nanoreactors. *Biomacromolecules* **2014**, *15* (7), 2389–2397. https://doi.org/10.1021/bm500127g.

(50) Hadjichristidis, N.; Iatrou, H.; Pitsikalis, M.; Sakellariou, G. Synthesis of Well-Defined Polypeptide-Based Materials via the Ring-Opening Polymerization of α-Amino Acid N-Carboxyanhydrides. *Chem. Rev.* **2009**, *109* (11), 5528–5578. https://doi.org/10.1021/cr900049t.

(51) Deming, T. J. Polypeptide and Polypeptide Hybrid Copolymer Synthesis via NCA

Polymerization. *Adv. Polym. Sci.* **2006**, *202* (1), 1–18. https://doi.org/10.1007/12_080.

(52) Tian, H.; Tang, Z.; Zhuang, X.; Chen, X.; Jing, X. Biodegradable Synthetic Polymers: Preparation, Functionalization and Biomedical Application. *Prog. Polym. Sci.* **2012**, *37* (2), 237–280. https://doi.org/https://doi.org/10.1016/j.progpolymsci.2011.06.004.

(53) Liu, Y.; Maruyama, T.; Biplab, K. C.; Mori, T.; Katayama, Y.; Kishimura, A. Inducible Dynamic Behavior of Polyion Complex Vesicles by Disrupting Charge Balance. *Chem. Lett.* **2021**, *50* (5), 1034–1037. https://doi.org/10.1246/cl.210037.

(54) Olson, F.; Hunt, C. A.; Szoka, F. C.; Vail, W. J.; Papahadjopoulos, D. Preparation of Liposomes of Defined Size Distribution by Extrusion through Polycarbonate Membranes. *Biochim. Biophys. Acta - Biomembr.* **1979**, *557* (1), 9–23. https://doi.org/https://doi.org/10.1016/0005-2736(79)90085-3.

(55) Kunz, D.; Thurn, A.; Burchard, W. Dynamic Light Scattering from Spherical Particles. *Colloid Polym. Sci.* **1983**, *261* (8), 635–644. https://doi.org/10.1007/BF01415033.

(56) Goto, A.; Yen, H. C.; Anraku, Y.; Fukushima, S.; Lai, P. S.; Kato, M.; Kishimura, A.; Kataoka, K. Facile Preparation of Delivery Platform of Water-Soluble Low-Molecular-Weight Drugs Based on Polyion Complex Vesicle (PICsome) Encapsulating Mesoporous Silica Nanoparticle. *ACS Biomater. Sci. Eng.* **2017**, *3* (5), 807–815. https://doi.org/10.1021/acsbiomaterials.6b00562.

(57) Kokuryo, D.; Anraku, Y.; Kishimura, A.; Tanaka, S.; Kano, M. R.; Kershaw, J.; Nishiyama, N.; Saga, T.; Aoki, I.; Kataoka, K. SPIO-PICsome: Development of a Highly Sensitive and Stealth-Capable MRI Nano-Agent for Tumor Detection Using SPIO-Loaded Unilamellar Polyion Complex Vesicles (PICsomes). *J. Control. Release* **2013**, *169* (3), 220–227. https://doi.org/10.1016/j.jconrel.2013.03.016.

(58) Kuhlman, P.; Duff, H. L.; Galant, A. A Fluorescence-Based Assay for Multisubunit DNA-Dependent RNA Polymerases. *Anal. Biochem.* **2004**, *324* (2), 183–190. https://doi.org/10.1016/j.ab.2003.08.038.

Graphical abstract

- Series of PEO-*b*-poly(*L*-Glu$_x$-*co*-*L*-Phe$_y$) and PEO-*b*-poly(*L*-Lys$_x$-*co*-*L*-Phe$_y$) PEO-copolypeptides with pH-sensitivity shown by CD profiles
- Hydrophobic *L*-Phe co-monomer influences 2ndary structure and shifts effective pKa
- Co-assembly of PEO-copolypeptides of same amino acid numbers x and y forms PICsomes stable in isotonic NaCl thanks to π-π stacking of *L*-Phe
- Encapsulation of duplex-firefly siRNA shows luciferase gene silencing in HeLa cells superior to lipofectamine™ polyplex

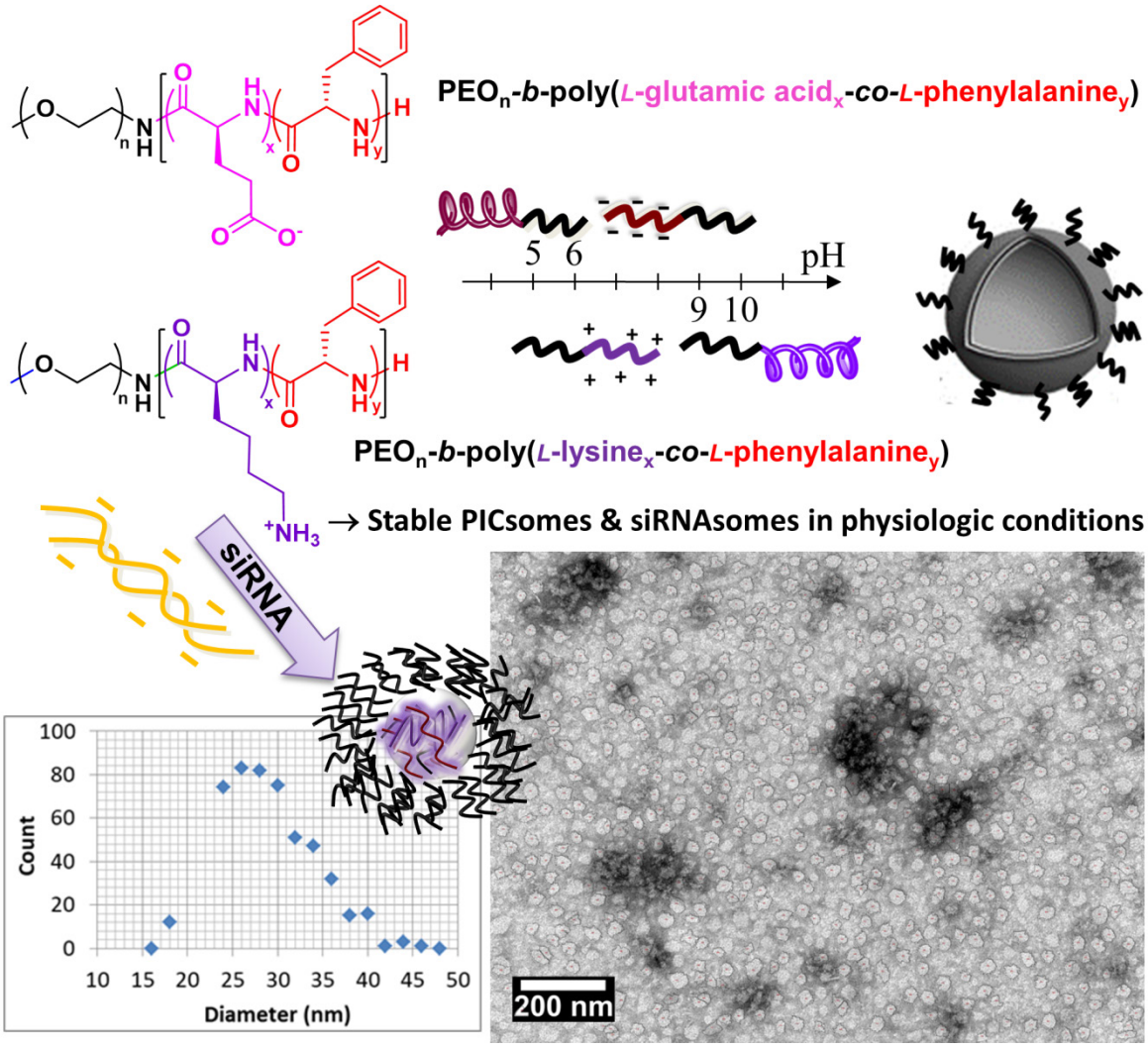

Supplementary data for:

Robust polyion complex vesicles (PICsomes) based on PEO-*b*-poly(amino acid) copolymers combining electrostatic and hydrophobic interaction: formation, siRNA loading and intracellular delivery

Esra Aydinlioglu [1], Mona Abdelghani [2], Gaëlle Le Fer [1,3], Jan C. M. van Hest [2], Olivier Sandre [1,] and Sébastien Lecommandoux [1,*]*

1 Univ. Bordeaux, CNRS, Bordeaux INP, UMR 5629 Laboratoire de Chimie des Polymères Organiques (LCPO), ENSCBP 16 avenue Pey Berland, 33607 Pessac, France

2 Department of Biomedical Engineering, Institute for Complex Molecular Systems (ICMS), Eindhoven University of Technology, PO Box 513, 5600 MB Eindhoven, The Netherlands

3 Univ. Lille, CNRS, INRAE, Ecole Centrale, UMR 8207 Unité Matériaux Et Transformations (UMET), Ingénierie des Systèmes Polymères (ISP) team, 59000 Lille, France

* Correspondence: olivier.sandre@enscbp.fr, lecommandoux@enscbp.fr

Example of characterization of poly(ethylene oxide)$_n$-b-poly(L-glutamic acid$_x$-co-L-phenylalanine$_y$) with ^{1}H NMR and SEC

As an example, the ^{1}H NMR spectra of PEO$_{46}$-*b*-poly(*L*-BLG$_{62}$-*co*-*L*-Phe$_{42}$ in *d*-TFA and of the corresponding unprotected copolymer PEO$_{46}$-*b*-poly(*L*-Glu$_{62}$-*co*-*L*-Phe$_{42}$ in *d*-DMSO are shown in Figure S1A and S1B respectively, and fully assigned. The degrees of polymerization (DP) of *L*-BLG and *L*-Phe units within the copolypeptide block in PEO$_n$-*b*-poly(*L*-BLG$_x$-*co*-*L*-Phe$_y$) were calculated to be x=62 and y=42, respectively, by comparing the integration of the peak at 5.35 ppm corresponding to the resonance of the methylene group (−COC**H$_2$**−) at the α position of the benzyl ring (2 ^{1}H per BLG unit) and the integration of the peak at 3.12 ppm corresponding to the resonance of the methylene group (C$_6$H$_5$− C**H$_2$**−) at the α position of the benzyl ring (2 ^{1}H per Phe unit) to the integral of the peak at 3.99 ppm of the methylene group of PEO (*vide supra*, 184 ^{1}H). The *L*-Phe (%) weight fractions of the final copolymer chains were calculated by dividing the molar mass of all phenylalanine moieties incorporated in the chains calculated by ^{1}H NMR (y × 147.2 g·mol^{-1}) to the $\overline{M_n}$ value of PEO$_n$-*b*-poly(*L*-Glu$_x$-*co*-*L*-Phe$_y$) after complete deprotection (here 16,200 g·mol^{-1}), as confirmed by the disappearance of the signal corresponding to the methylene group of the BLG units in α of the removed benzyl ring (Figure S1B).

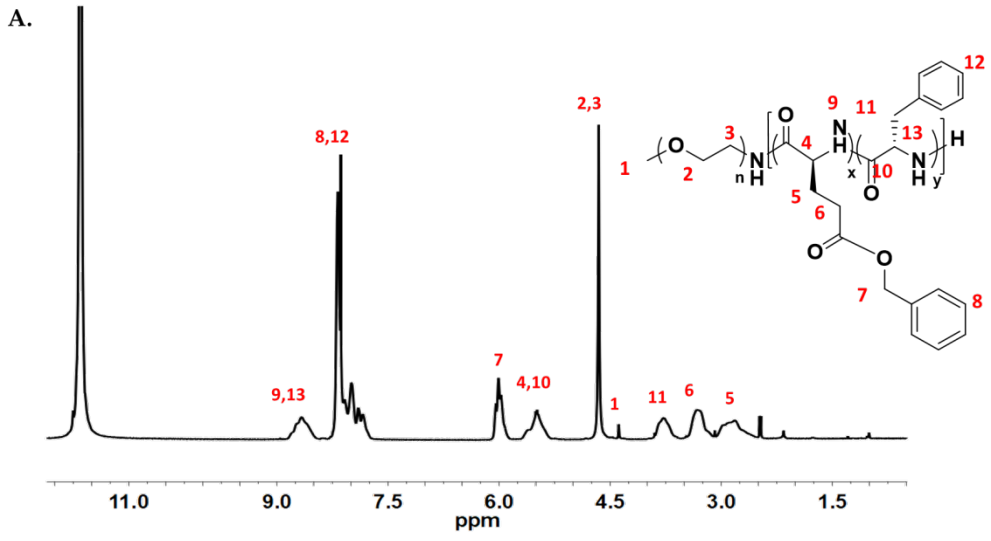

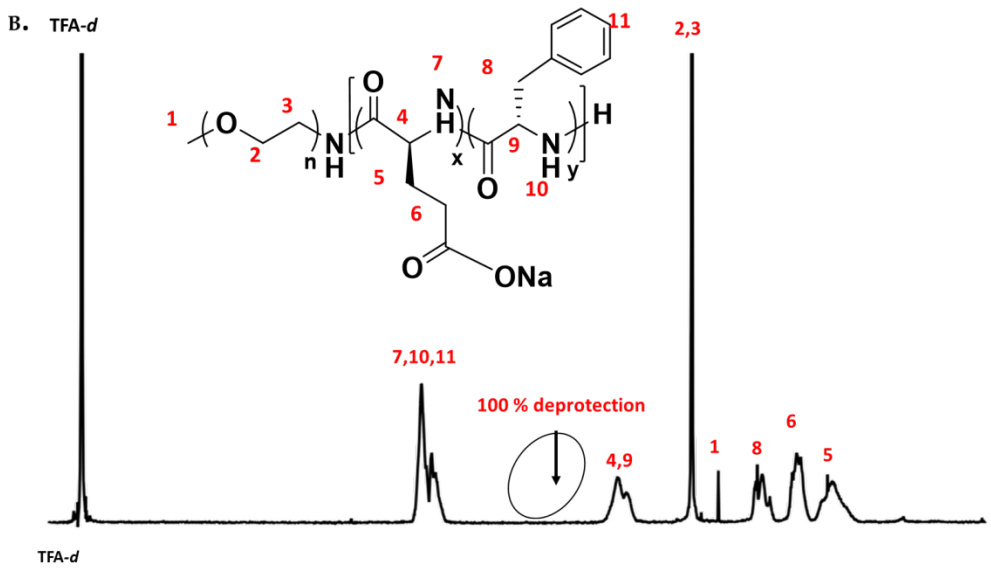

Figure S1. A) Representative ^{1}H NMR spectrum of PEO$_{46}$-*b*-poly(*L*-BLG$_{62}$-*co*-*L*-Phe$_{42}$) in *d*-TFA and B) of PEO$_{46}$-*b*-poly(*L*-Glu$_{62}$-*co*-*L*-Phe$_{42}$) in *d*-DMSO after deprotection.

Characterization of poly(ethylene oxide)$_n$-b-poly(L-glutamic acid$_x$-co-L-phenylalanine$_y$) by size exclusion chromatography

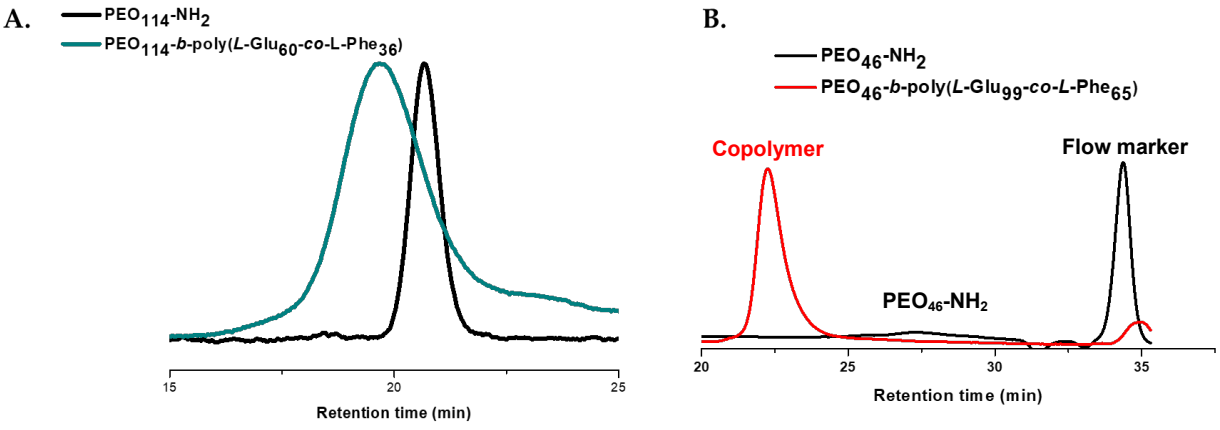

Figure S2. Size exclusion chromatography profiles of **A)** PEO$_{114}$-*b*-poly(*L*-BLG$_x$-*co*-*L*-Phe$_y$) before deprotection) in DMF + 0.1% LiBr *via* polystyrene calibration with RI detector**. B)** PEO$_{46}$-*b*-poly(*L*-BLG$_x$-*co*-*L*-Phe$_y$) (after deprotection) in DMSO (0.5 mL·min^{-1}) at 80 °C in the presence of LiBr (1 g L^{-1}) with an RI detector and dextran used as a calibration standard.

Characterization of poly(ethylene oxide)$_n$-b-poly(L-Lysine$_x$-co-L phenylalanine$_y$) with ^{1}H NMR and SEC

^{1}H NMR spectra of PEO$_{114}$-*b*-poly(*L*-Lys(TFA)$_{52}$-*co*-*L*-Phe$_{20}$) in *d*-TFA and of the corresponding copolymer PEO$_{114}$-*b*-poly(*L*-Lys$_{52}$-*co*-*L*-Phe$_{20}$) are shown in Figure S1 and S2 respectively, and fully assigned. The degrees of polymerization (DP) of *L*-Lys(TFA) and *L*-Phe units within the copolypeptide block in PEO-*b*-poly(*L*-Lys-*co*-*L*-Phe) were calculated to be 52 and 20, respectively, by comparing the integration of the peaks between 0.77 to 1.54 ppm corresponding to the resonance of the methylene group (−C**H$_2$**−C**H$_2$**−C**H$_2$**−C**H$_2$**−NH− of lysine (β, γ, δ-methylene protons of the lysine side chains) (6 ^{1}H per Lys unit) and the integration of the peak at 2.35 ppm corresponding to the resonance of the methylene group (C_6H_5− C**H$_2$**−) at the α position of the benzyl ring (2 ^{1}H per Phe unit) to the integral of the peak at 3.15 ppm of the methylene group of PEO (*vide supra*, 456 ^{1}H). The M_n value of PEO-*b*-poly(*L*-Lys-*co*-*L*-Phe) calculated by ^{1}H NMR is 22,777 g·mol^{-1}. Complete deprotection was confirmed by the shifting of the signal corresponding to the peak of lysine at 3.20 ppm to 2.74 ppm (−C**H$_2$**−NH− of lysine). While poly(*L*-Lysine (TFA) blocks exhibit a secondary structure (α-helix or β-sheet) through hydrogen bonding between CO and NH groups, poly(*L*-lysine) chains probably adopt a coil-like conformation after deprotection. This conformational transition was characterized by a shift of the ε-methylene protons of the lysine side chains from δ = 3.20 ppm to δ = 2.74 ppm in the ^{1}H NMR spectra (Figure S3).

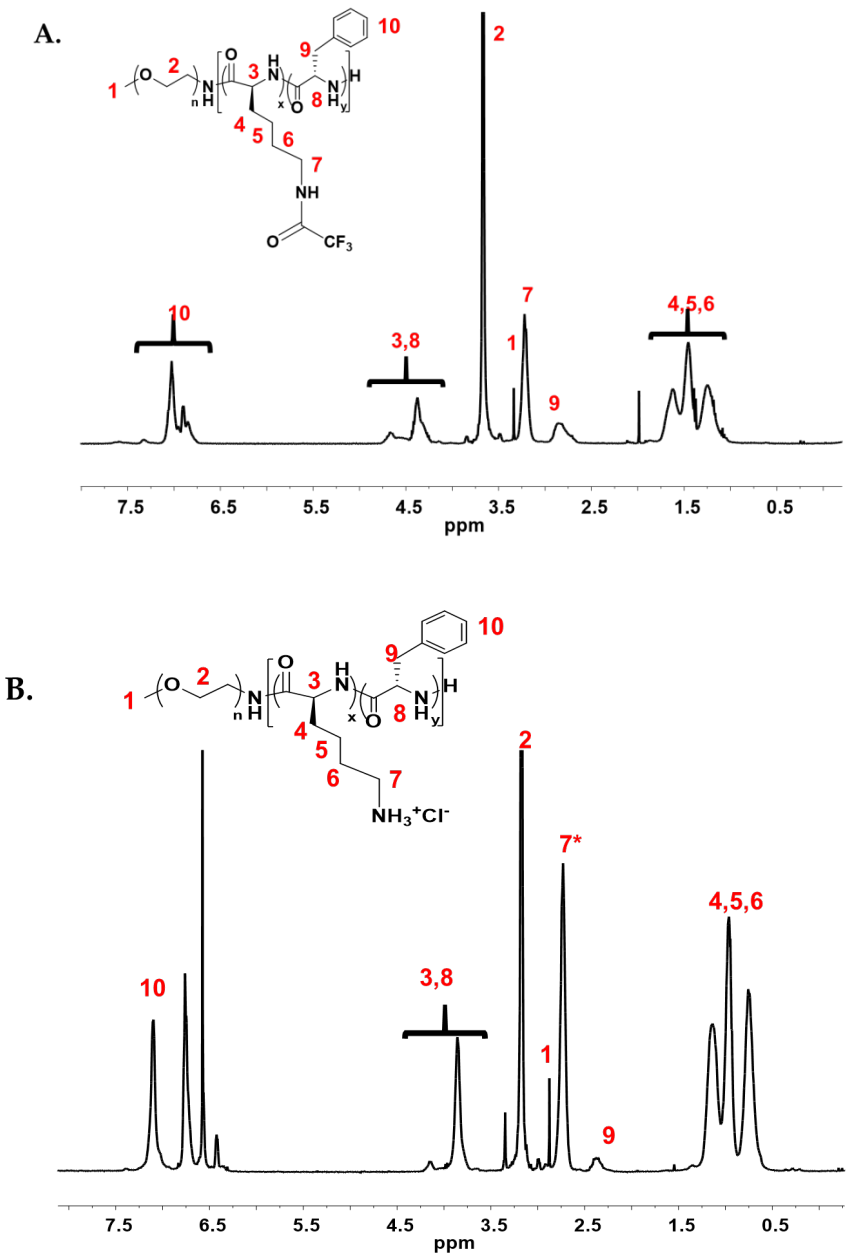

Figure S3. A) ^{1}H NMR spectrum of PEO_{114}-*b*-P(*L*-Lys(TFA)$_{52}$-*co*-*L*-Phe_{20}) in TFA-*d* (before deprotection). B) ^{1}H NMR spectrum of PEO_{114}-*b*-P(*L*-Lys_{52}-*co*-*L*-Phe_{20}) in $CDCl_3$+TFA (20 %) (after deprotection).

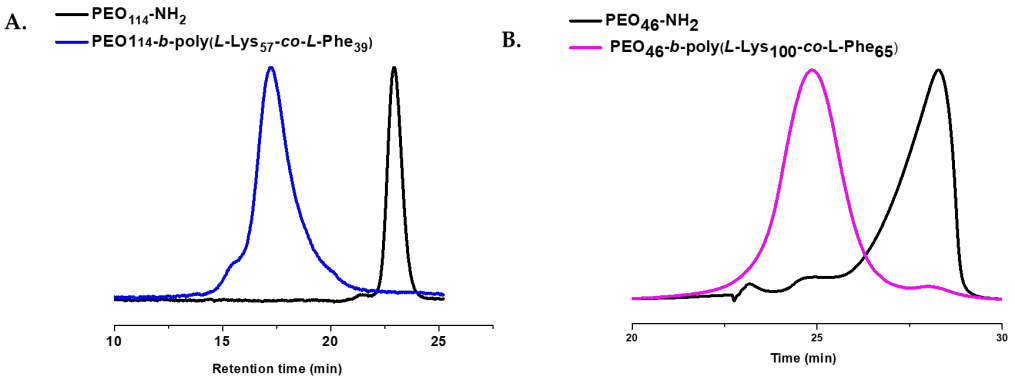

Figure S4. A) Normalized size exclusion chromatography profiles of PEO_{114}-*b*-poly(*L*-Lys-TFA_x-*co*-*L*-Phe_y) (before deprotection) in DMF + 0.1% LiBr *via* polystyrene calibration with RI detector. B) Normalized size exclusion chromatography profiles for PEO_{46}-*b*-poly(*L*-Lys_x-*co*-*L*-Phe_y) (before deprotection) in DMF + 0.1% LiBr *via* polystyrene calibration with RI detector.

Formation of PEO_{114}–based ionic complexations

Table S1. Summary of results at different charge ratios after formation of polyionic complexes for PEO_{114}–based copolymers as determined by DLS and zetametry (NA: non-available)

Ratio [NH_3^+/COO^-]	D_h (nm)	PDI	Derived countrate kcps	ζ potential (mV)
0.1:1	210	0.3	137	NA
0.5:1	170	0.3	481	-2±4
1:1	197	0.34	700	NA
1:1 extruded	230	0.29	687	0.7±3

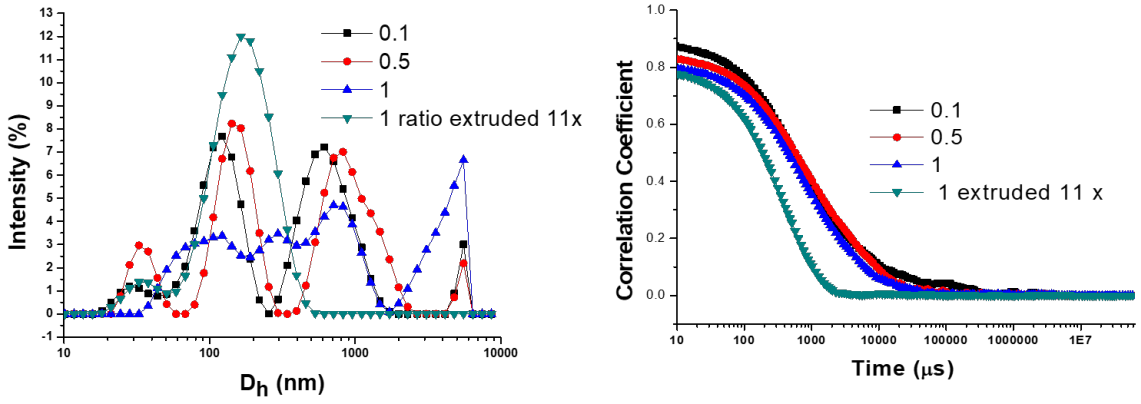

Figure S5. Size distribution profiles of PICsomes formed by PEO_{114}–based copolymers at different charge ratios determined by DLS measurements (Malvern NanoZS, 90°).

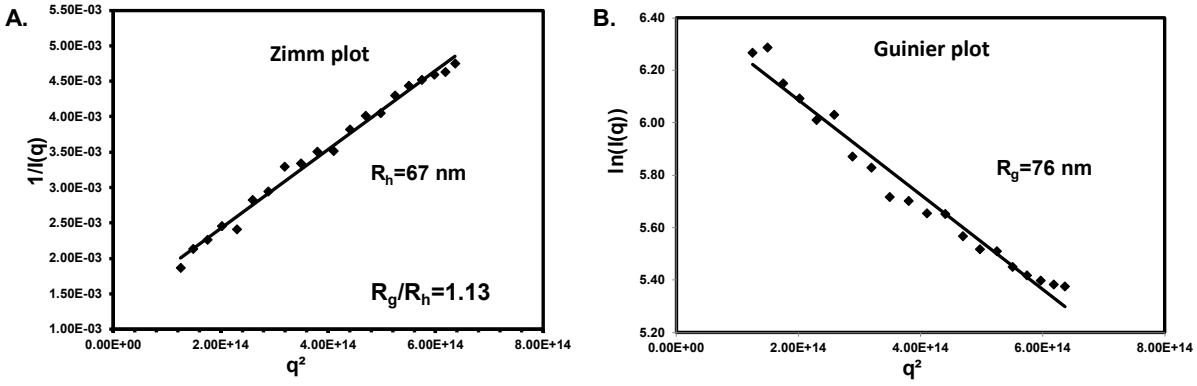

Figure S6. Multi-angle light scattering analysis of PICsomes at 1:1 charge ratio prepared from the lower *f*-PEO ratio PEO_{46}–copolypeptides. A) Variation of decay rate *vs.* squared scattering vector and R_h determination; B) Guinier plot for R_g determination.

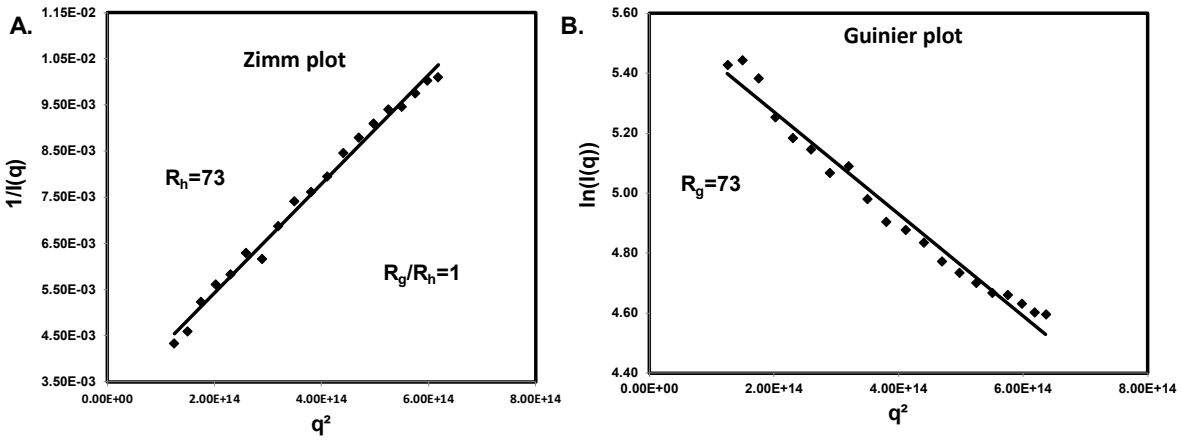

Figure S7. Multi-angle light scattering analysis of PICsomes at 1:1 charge ratio prepared from the higher *f*-PEO (%) ratio PEO_{114}–copolypeptides after extrusion. A) Variation of decay rate *vs.* squared scattering vector and R_h determination; B) Guinier plot for R_g determination.

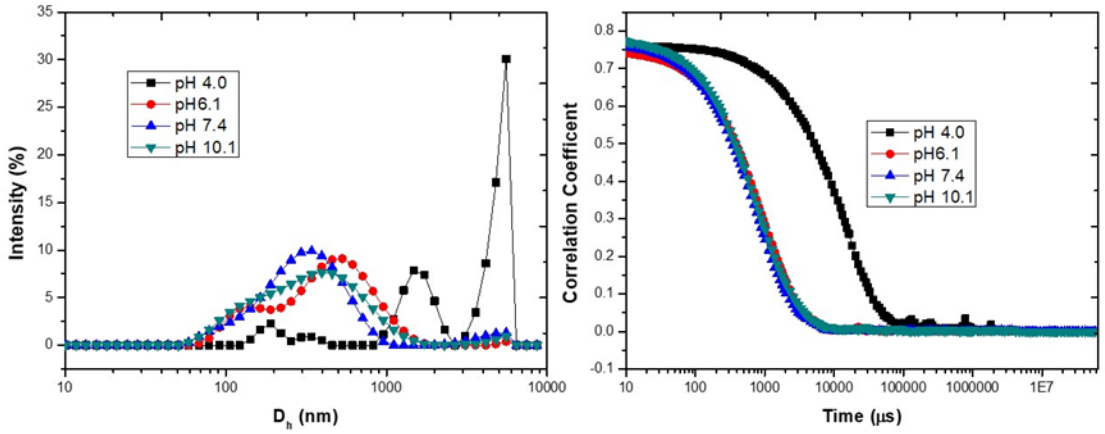

Figure S8. Size distribution profiles for the pH responsiveness of PICsomes formed from PEO_{46}–based copolymers at varying pH values.

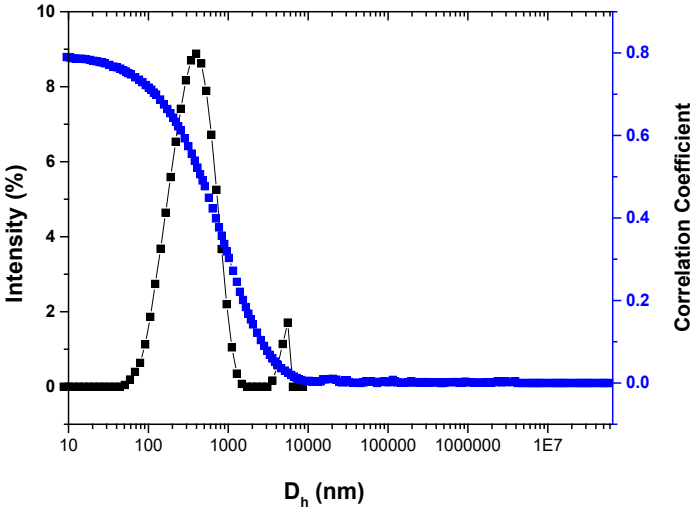

Figure S9. Dynamic light scattering analysis of empty PICsomes at *Z*=1 charge ratio prepared from PEO_{46}–based copolymers in serum media (in Opti-MEM at 37° C).

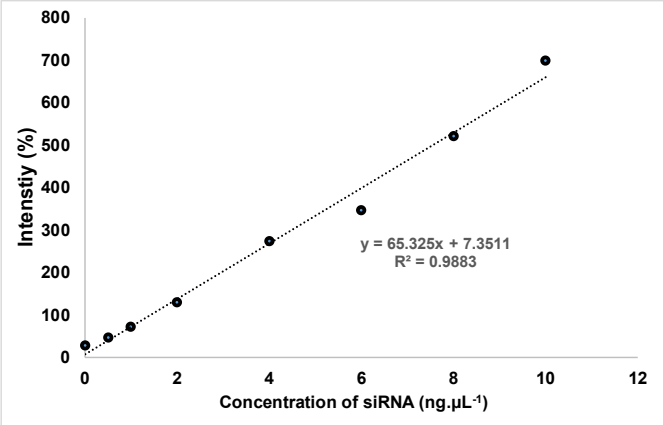

Figure S10. Standard calibration curve of fluorescence signal at different siRNA concentrations obtained from Quant-iT™ RiboGreen™.